Geochimica et Cosmochimica Acta 355 (2023) 210–221

Contents lists available at ScienceDirect

Geochimica et Cosmochimica Acta

journal homepage: www.elsevier.com/locate/gca

Position-specific carbon isotopes of Murchison amino acids elucidate extraterrestrial abiotic organic synthesis networks

Sarah S. Zeichner [a,*], Laura Chimiak [a,b], Jamie E. Elsila [c], Alex L. Sessions [a], Jason P. Dworkin [c], José C. Aponte [c], John M. Eiler [a]

[a] Division of Geological & Planetary Sciences, California Institute of Technology, Pasadena, CA 90025, USA
[b] Department of Geological Sciences, UCB 399, University of Colorado, Boulder, CO 80309, USA
[c] Solar System Exploration Division, Code 691, NASA Goddard Space Flight Center, Greenbelt, MD 20771, USA

ARTICLE INFO

Associate editor: Yoko Kebukawa

Original content: MurchisonAminoAcids (Original data)
MurchisonAminoAcids (Original data)

Keywords:
Isotope geochemistry
Meteoritic organics
Orbitrap mass spectrometry

ABSTRACT

The Murchison meteorite is a well-studied carbonaceous chondrite with relatively high concentrations of amino acids thought to be endogenous to the meteorite, in part because they are characterized by carbon isotope ($\delta^{13}C$) values higher than those typical of terrestrial amino acids. Past studies have proposed that extraterrestrial amino acids in the Murchison meteorite could have formed by Strecker synthesis (for α-amino acids), Michael addition (for β-amino acids), or reductive amination, but a lack of constraints have prevented confident discrimination among these possibilities, or assignment of specific formation pathways to each of several specific amino acids. Position-specific carbon isotope analysis differentiates amongst these mechanisms by relating molecular sites to isotopically distinct carbon sources and by constraining isotope effects associated with elementary chemical reactions. Prior measurements of the position-specific carbon isotopic composition of α-alanine from the Murchison CM chondrite demonstrated that alanine's high $\delta^{13}C_{VPDB}$ value is attributable to the amine carbon ($\delta^{13}C_{VPDB} = +142 \pm 20‰$), consistent with Strecker synthesis drawing on ^{13}C-rich carbonyl groups in precursors (Chimiak et al., 2021). Here, we measured the $\delta^{13}C$ composition of fragment ions generated by electron impact ionization of derivatized α-alanine, β-alanine, and aspartic acid from Murchison via gas chromatography-Fourier transform mass spectrometry. α-Alanine's amine carbon yielded $\delta^{13}C_{VPDB} = +109 \pm 21‰$, which is consistent with the previously measured value and with formation from ^{13}C-rich precursors. β-Alanine's amine carbon presents a lower $\delta^{13}C_{VPDB} = +33 \pm 24‰$, which supports formation from ^{13}C-rich precursors but potentially via a Michael addition mechanism rather than Strecker synthesis. Aspartic acid's amine carbon has $\delta^{13}C_{VPDB} = -14 \pm 5‰$, suggesting synthesis from precursors distinct from those that generated the alanine isomers. These measurements indicate that Murchison amino acids are a mixture of compounds made from different synthesis mechanisms, though some subsets likely drew on the same substrates; this conclusion highlights the complexity of extraterrestrial organic synthesis networks and the potential of emerging methods of isotope ratio analysis to elucidate the details of those networks.

1. Introduction

Carbonaceous chondrites are amongst the most primitive materials in the Solar System, with heterogeneous compositions representing a diverse range of sources and formation processes spanning environments from the Interstellar Medium (ISM) to the Solar Nebula. Carbonaceous chondrites have up to 3 weight % organic carbon; studying these organic molecules can provide insights into prebiotic synthesis, potential sources of organic compounds on early Earth, and a framework for interpreting the origins of organic compounds that are the target of extraterrestrial sample return missions (Glavin et al., 2018). In particular, the Murchison meteorite is an ideal specimen for studying extraterrestrial organics. Murchison is a hydrated Mighei-type (CM2) meteorite that fell in 1969 near Murchison, Australia (Seargent, 1990), and has since been extensively studied due to its availability and relatively high concentration and chemical diversity of soluble organic compounds such as amino acids (review of studies in Glavin et al., 2018).

* Corresponding author.
E-mail address: szeichner@caltech.edu (S.S. Zeichner).

https://doi.org/10.1016/j.gca.2023.06.010
Received 20 January 2023; Accepted 11 June 2023
Available online 14 June 2023

The abiotic synthesis of amino acids is of particular interest in origins of life research due to their biological ubiquity. Several pathways can synthesize amino acids abiotically; most require relatively complex series of reactions operating under specific conditions, imposing constraints on formation of these molecules on early Earth and the extraterrestrial settings where amino acids are found (Pizzarello et al., 2006; Glavin and Dworkin, 2009; Elsila et al., 2016; Glavin et al., 2020b). More than 90 amino acids have been identified in the Murchison meteorite, including proteinogenic ones (e.g., glycine, alanine, aspartic acid; Pizzarello et al., 2006; Glavin and Dworkin, 2009; Elsila et al., 2016; Glavin et al., 2020b). The presence of non-proteinogenic amino acids, rare isotope enrichments in molecular average H-, N-, and C-compositions of meteoritic amino acids versus terrestrial biological amino acids (Table S5), and near-racemic mixtures of D/L enantiomers present compelling evidence that these amino acids are mostly endogenous to the Murchison meteorite (Pizzarello et al., 2004; Burton et al., 2012; Elsila et al., 2016).

A range of hypotheses exist regarding the reactions that could have synthesized α-, β-, γ-, δ-, etc. amino acids found in carbonaceous chondrites (summarized in Elsila et al., 2012; Chimiak and Eiler, 2022, among others): Fischer Tropsch/Haber Bosch-type synthesis (FTT-type; Hayatsu et al., 1971; Kress and Tielens, 2001; Botta and Bada, 2002; Burton et al., 2012), Strecker-Cyanohydrin-type synthesis to form α-amino acids (Peltzer et al., 1984), coupled with formaldehyde addition to form more complex soluble organic molecules (Chimiak and Eiler, 2022), ammonia involved formose reaction (Koga and Naraoka, 2017), reductive amination (Huber and Wächtershäuser, 2003), and Michael addition to form β-amino acids (Miller, 1957). Many of these processes require the presence of water and thus would likely occur in the meteorite parent body, but could form from precursors originally deriving from the ISM; amino acids could also potentially form in-situ within the protosolar nebula or ISM via UV irradiation of ice grains (Bernstein et al., 2002; Muñoz Caro et al., 2002), although evidence for interstellar amino acids remains contested.

Structurally distinct groups of amino acids are expected to form via distinct pathways, so it seems likely that some combination of the preceding processes contributed to formation of the observed compounds (Sephton, 2002; Pizzarello et al., 2004; Burton et al., 2012; Elsila et al., 2016). However, it is unclear which process or processes dominate production of any specific amino acid, or whether different formation pathways occurred together, drawing on common substrates, or instead occurred independently from different pools of substrates.

Prior measurements of compound-specific carbon isotopic compositions of Murchison amino acids reveal many of them to be ^{13}C-enriched (Sephton, 2002; Pizzarello et al., 2006; Glavin and Dworkin, 2009). For instance, α-alanine from the Murchison meteorite has been measured previously, yielding $\delta^{13}C_{VPDB}$ values of +25‰ to +52‰ (for either the D or the L enantiomer or a mixture of the two; Table S5; see Eq. (1) for definition of δ). These values are higher than those typical of terrestrial biogenic alanine ($\delta^{13}C_{VPDB}$ usually < -20‰ but with values as high as −11‰ in C-4 plants; Cerling et al., 1997; Rasmussen and Hoffman, 2020). ^{13}C-enrichment suggests that synthesis of Murchison amino acids drew on precursors synthesized in the ISM. Interstellar molecules such as CO preferentially bond with heavier isotopes (i.e., ^{13}C; Charnley et al., 2004) relative to the population of free atoms, ions and radicals at cold temperatures (~10 K; Öberg, 2016; Jørgensen et al., 2018), a process driven by the greater thermodynamic stability of molecules that contain a heavy isotope. This process can be modeled by the following exothermic reaction – $^{12}CO + {}^{13}C^{+} \Leftrightarrow {}^{13}CO + {}^{12}C^{+}$ – where ^{13}C is thought to preferentially be sequestered within CO due to enhanced stability of the C–C bond at low temperatures. Interstellar hydrocarbons are formed from the reaction of C^{+} with hydrogen, and are therefore thought to not be subject to such extreme stabilization of heavy-isotope substituted products, and thus are expected to be relatively ^{13}C-depleted.

However, it is challenging to make more specific interpretations of prior C isotope data of meteoritic amino acids. Molecular-average or "compound-specific" isotope analyses (CSIA) are limited in what they can reveal about mechanisms of amino acid synthesis, as the averaging across molecular sites can confound the effects of several variables (e.g., precursor isotopic compositions; reaction mechanisms; parent body processing; secondary alteration) on the isotopic composition.

Position-specific stable isotope analysis (PSIA) of meteoritic amino acids provides an opportunity to directly test abiotic synthesis hypotheses by tracing the isotopic compositions of putative precursor molecules to specific positions within reaction products. Prior studies have leveraged the potential of PSIA to understand reaction mechanisms for the formation of biological organics (e.g., (Abelson and Hoering, 1961; DeNiro and Epstein, 1977; Monson and Hayes, 1980; Melzer and O'Leary, 1987), but until recently PSIA has required either chemical cleavage to isolate specific sites into molecules easily convertible into CO_2 for measurement via traditional isotope-ratio-mass-spectrometry methods, or NMR measurements of large samples (100s of mg) of pure analytes. The gas chromatography (GC)-Orbitrap is an emerging technology that enables precise, high-mass-resolution isotope measurements of relatively small samples (~μg and less) to record some features of position-specific isotopic variations in amino acids (and other molecules), where many compounds within a complex mixture can be introduced (following derivatization), subjected to an online separation and subsequently analyzed. The GC-Orbitrap platform enables measurements of position-specific isotopic composition by fragmenting analyte molecules in the ion source (Fig. 1). Individual fragments subsample different combinations of molecular positions, such that several measured together may constrain differences in the rare isotope contents of different atomic sites of the parent molecule (Fig. 2).

We previously applied this technique to constrain the carbon isotopic composition of α-alanine from Murchison using PSIA (Chimiak et al., 2021). We demonstrated that in the Murchison specimen analyzed, the high molecular-average $\delta^{13}C$ value (+26‰) was derived from a ^{13}C-enriched amine carbon (+142 ± 20‰), and diluted by ^{13}C-depleted compositions for the carboxyl and methyl carbons (−29 ± 10‰ and −36 ± 20‰, respectively; Chimiak et al., 2021). Position-specific $\delta^{13}C$ values from Chimiak et al., 2021 suggest that Murchison α-alanine inherits the ^{13}C-enrichment in its amine carbon from a distinct, isotopically heavy carbon precursor (hypothesized to be carbonyl groups in aldehydes, which are suggested to derive from CO in the ISM), whereas the other two carbons are inherited from more ^{13}C-depleted precursors, either from ^{13}C-poor compounds in the ISM (e.g., hydrocarbons or HCN) or from carbon sources on the meteorite parent body (e.g., HCN; $\delta^{13}C_{VPDB}$ of KCN in Murchison = 5 ± 3‰; Pizzarello, 2014; $\delta^{13}C_{VPDB}$ of cometary HCN = 16^{+262}_{-172}‰; Cordiner et al., 2019; Chimiak et al., 2021).

We argued that these precursors formed α-alanine (and other α-amino acids) via Strecker synthesis, plausibly in the meteorite parent body. However, this measurement and hypothesized reaction mechanism cannot provide constraints on how amino acids other than α-amino acids may have formed, and how the various classes of amino acids found in meteorites relate to one another. Performing PSIA on a several amino acids of distinct structural groups within the same sample presents an opportunity to relate position-specific isotopic compositions of amino acids, and their respective plausible formation pathways, to each other.

Here, we present measurements of position-specific carbon isotope values of α-alanine, aspartic acid, and β-alanine from Murchison and use our results to make specific assignments of the most plausible formation mechanisms for each of the measured amino acids. Many of these mechanisms have been introduced in prior studies (e.g., Elsila et al., 2012; Simkus et al., 2019b); we build upon these hypotheses with numerical constraints on isotope effects that serve to connect our position-specific isotope values with the isotopic compositions of potential precursors, thus building quantitative arguments in support of the most plausible reaction pathways. Our posited mechanisms offer a pathway

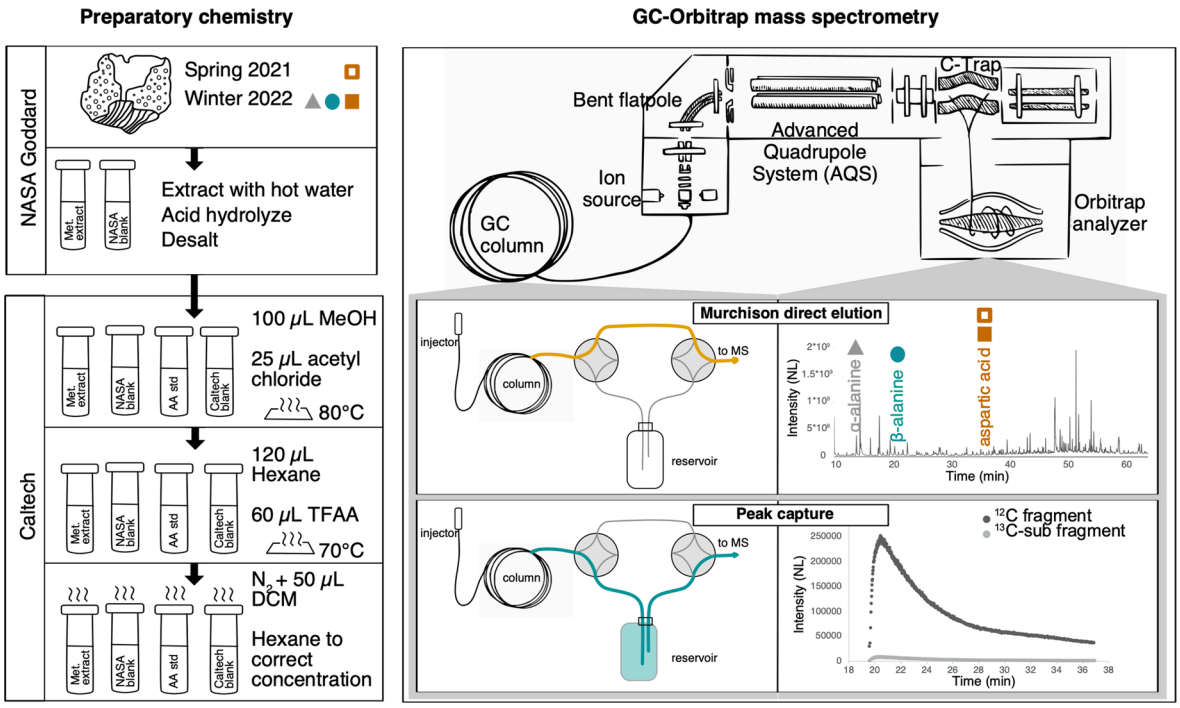

Fig. 1. Preparatory chemistry and Orbitrap mass spectrometry. (left, Preparatory chemistry) Meteorite (Met.) samples were extracted, hydrolyzed, and desalted at NASA Goddard, before being sent to Caltech and derivatized in parallel with amino acid standards (AA std) and procedural blanks for introduction into the GC Orbitrap. (right, GC-Orbitrap mass spectrometry) GC-Orbitrap instrumental setup. Samples are introduced via gas chromatography into the mass spectrometer, where compounds are ionized, accelerated through the bent-flatpole, and mass-separated in the quadrupole before being stored in the C-trap, and injected into the Orbitrap. Two valves within the GC are used to direct the effluent through an internal plumbing that enable two types of measurements: direct elution and peak capture. Direct elution measurements allow the user to optimize chromatography and identify peak elution timing (Zeichner et al., 2022), while peak capture measurements capture a single fragment of interest within a stainless-steel reservoir and allow it to slowly purge into the MS over time.

for structurally distinct classes of amino acids to be synthesized from a small number of initial substrates, providing support for the hypothesis that a complex network of extraterrestrial organic synthesis created diverse amino acids from a common set of simple precursors. In particular, the doubly-carboxylated aspartic acid and the β-amino acid β-alanine have structural properties that differ from α-alanine and each other and cannot rely only on a Strecker synthesis mechanism as proposed for α-alanine's formation. PSIA allows us to distinguish the most plausible mechanisms for β-alanine and aspartic acid from a range of other mechanisms, in a way that cannot be resolved using CSIA alone.

2. Methods

2.1. Meteorite samples and amino acid standards

We analyzed two specimens of the Murchison meteorite – a 1.7 g piece (Spring 2021) with some known terrestrial contamination and a 1.5 g piece (Winter 2022) with evidence of minimal terrestrial contamination (Friedrich et al., 2019). The specimens were both acquired from the Field Museum of Natural History and previously described by Friedrich et al., 2019. Both samples were prepared via the same hydrolysis and desalting procedure at NASA Goddard Space Flight Center (GSFC) following the protocol from Elsila et al. (2012), along with a procedural blank prepared in parallel to confirm that no organics were being introduced during preparatory chemistry (Table S4).

Briefly, each sample was ground to a homogenized powder. The powder was split into two portions for more efficient extraction and then sealed in a glass ampoule with 1 mL of ultrahigh purity water (Millipore Integral 10 UV, 18.2 MX cm, <3 ppb total organic carbon) for 24 hours at 100 °C. The water extract was separated, dried under vacuum, and hydrolyzed in 6 N HCl vapor (Tamapure-AA-10 purity, Tama Chemicals) for 3 hours at 150 °C. This hydrolyzed extract was then desalted on a cation-exchange resin column (AG50W-X8, 100–200 mesh, hydrogen form, Bio-Rad), with the amino acids recovered by elution with 2 M NH_4OH (prepared from ultrahigh purity water and NH_3 (g) *in vacuo*) and dried under N_2. The Spring 2021 specimen was processed in this way in March 2021 and the Winter 2022 specimen in September of 2021 (Fig. 1).

The abundances of amino acid enantiomers of both the Spring 2021 and Winter 2022 specimens were measured at GSFC via liquid chromatography with fluorescence detection and time-of-flight mass spectrometry (LC-FD/ToF- MS) using methods described in Glavin et al. (2010). Following LC-FD/ToF-MS analysis, the extracts were sent separately to Caltech along with a GSFC analytical blank processed in parallel. Upon arrival at Caltech, both the Murchison extract and the GSFC analytical blank were stored in a freezer until analyses in April 2021 and January 2022, respectively.

For comparison to amino acids within meteorite extracts, we prepared pure amino acid standards of aspartic acid, β-alanine, and α-alanine, whose molecular average carbon isotopic composition ($\delta^{13}C_{VPDB} \pm 1s_{SE}$) were constrained by Elemental Analyzer-Isotope Ratio Mass Spectrometry at Caltech to be –22.14 ± 0.07‰ (n = 3), −27.09 ± 0.40‰ (n = 3) and −19.60 ± 0.24‰ (n = 3), respectively (Table S1). In addition to the pure extracts, we mixed unlabeled standards with a pure ^{13}C label at each site (10% label by mass; Supplemental Materials and Methods). This labeling experiment allowed us to identify fragments for each amino acid that sample a distinct combination of carbon positions to constrain each site, which can be converted into position-specific measurements (Section 2.5; Figs. 2 & S2).

2.2. Preparatory chemistry

Prior to analyses, meteorite extracts were redissolved in 1 mL of 3:1 H_2O:MeOH. After they were allowed to stand for 20 min, we sonicated

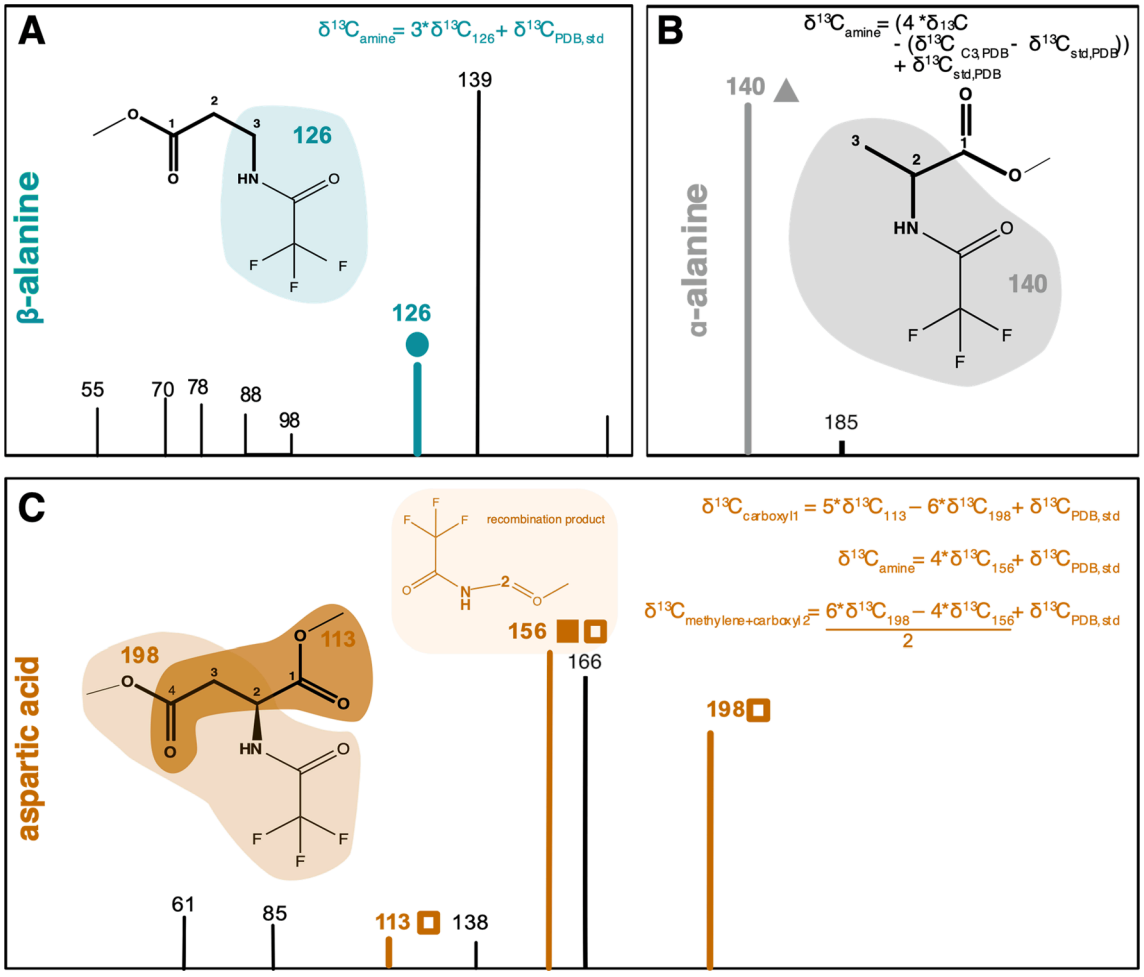

Fig. 2. Amino acid mass spectral fragments. Derivatized amino acids form characteristic fragments when introduced via GC into the electron impact source. These fragments can be used to independently constrain the isotopic composition of distinct combinations of carbon sites and calculate position-specific isotope ratios. Here, we depict fragmentation spectra of (**A**) β-alanine, (**B**) α-alanine, and (**C**) aspartic acid. The derivatized amino acid structure is inset within each figure, where the bolded part of the structure highlights the structure of the underivatized amino acid. Shaded areas illustrate the molecular geometry of mass spectral fragments of the original derivatized molecule that we measured within this study, although some fragments we measured were recombination products (e.g., 156 fragment of aspartic acid) and thus are depicted alongside the original molecular structure. Teal circles represent β-alanine measurements, grey triangles represent α-alanine measurements and burnt orange squares represent aspartic acid measurements. For peak capture measurements, each colored fragment was isolated within and slowly purged from the reservoir into the mass spectrometer over minutes to tens of minutes (Fig. 1). Fragment isotope ratios initially measured in comparison to the isotope ratio of house amino acid standards were converted into position-specific isotope ratios within a modeled PDB (mPDB*) reference frame using the equations presented within each of the panels (Section 2.4). (For interpretation of the references to colour in this figure legend, the reader is referred to the web version of this article.)

them for 10 min to ensure full dissolution and homogenization within the sample vial. The solutions were transferred to 2 μL GC vials for derivatization chemistry. Half of the Spring 2021 sample was derivatized for analysis, and the full Winter 2022 sample was derivatized. To ensure quantitative transfer of sample when the full sample was being used, sample vials were rinsed three times with 50 μL of MilliQ water, which was also transferred into the GC vial. At this stage, a second blank was introduced to trace any potential sources of contamination during the derivatization chemistry. Samples, standards, and blanks were dried down fully under N_2 and derivatized in parallel as follows (Fig. 1).

For analysis on the gas chromatograph (GC), we prepared derivatives by methylating the carboxyl group and trifluoroacetylating the hydroxyl and amine groups, producing N,O-bis(trifluoroacetyl) methyl esters (monoisotopic masses 257.05 Da, 199.05 Da, and 199.05 Da for aspartic acid, β-alanine, and α-alanine, respectively; Fig. 1). The derivatization protocols were adapted from Corr and others and performed at Caltech (Corr et al., 2007). The samples and standards within GC vials were dissolved in 100 μL of anhydrous methanol (Sigma Lots SHBK8757 and 8HBN2144 for the Spring 2021 and Winter 2022 samples, respectively). Standard vials were placed on ice, where 25 μL of acetyl chloride (Sigma Lots BCBW8067 and S6039952B0 for the Spring 2021 and Winter 2022 samples, respectively) was added dropwise. Vials were heated at 80 °C for 1 h, then gently dried under N_2. Samples were dissolved in 120 μL of hexane, and 60 μL of trifluoroacetic anhydride (TFAA; Sigma Lots SHBK5942 and S7307761110 for the Spring 2021 and Winter 2022 samples, respectively) added to the vials and heated at 110 °C for 30 min, after which they were briefly dried under N_2 until 25 μL of solvent remained in the vial. 100 μL of DCM was added to the vials to aide in eliminating residual derivatizing agent, then left to dry under N_2 until 10 μL were left. Derivatized standards were suspended in hexane (50 μL for samples and 1000 μL for standards). Standards were serially diluted to reach appropriate concentrations for introduction into the GC Orbitrap (i.e., 10s-100s pmols per 1 μL injection). Blanks were diluted in hexane to reach the same concentration of the meteorite samples. Samples, standards, and procedural blanks were derivatized in parallel but dried down separately to avoid cross contamination (Table S4).

2.3. Isotope analysis via GC-Orbitrap

Isotope analyses of amino acid mass spectral fragments were performed on a Q-Exactive Orbitrap mass spectrometer with samples introduced via a Trace 1310 GC equipped with a split/splitless injector operated in splitless mode with a TG-5SIL MS column (30 m (Spring 21) or 60 m (Winter 22), 0.25 mm ID, 0.25 μm film thickness) and a 1 m fused silica capillary pre-column (220 μm /363 μm VSD tubing; Fig. 1). Prior to position specific analyses of each amino acid, we performed direct elution measurements of samples and standards to confirm oven ramps, elution timing of each compound of interest, and detect any potential extraneous ions that co-eluted with analyte fragments within the mass window of interest (Figs. 1 & S1; Supplemental Materials and Methods; Zeichner et al., 2022). For the Spring 2021 sample, the following oven program was used: 50–85 °C by 10 °C per minute, 85–100 °C by 1 °C per minute with a 9 min hold, and 100–180 °C by 4 °C per minute with a 10 min hold. For the Winter 2022 sample, the following oven program was used: 50–85 °C by 10 °C per minute, 85–100 °C by 1 °C per minute with a 9 min hold, and 100–180 °C by 4 °C per minute with a 58 min hold. Special care was taken to optimize chromatography to ensure that amino acids of interest did not co-elute with nearby compounds, and that prior compound tails did not contribute mass fragments at abundances above baseline within the mass range for each measurement.

Following the optimization of GC conditions, we performed peak capture measurements using a Silco-coated stainless steel reservoir (10 cc; SilcoTek, Bellefonte, PA; Fig. 1; Eiler et al., 2017; Chimiak et al., 2021; Wilkes et al., 2022). We used valves to route the eluent into the reservoir during the elution time frame of the amino acid of interest (Fig. 1), thus capturing the compound such that we could slowly purge it into the Orbitrap to observe the fragments of interest for a longer period of time than traditional GC peaks (~minutes to tens of minutes instead of tens of seconds).

We performed Orbitrap measurements of the carbon isotope ratios of fragment ions of the derivatized amino acids by focusing the Advanced Quadrupole System (AQS) of the QExactive platform to mass windows 6.5 or 7 Da wide, centered around the mass of the unsubstituted mass spectral peak of each fragment. Focused mass window measurements reduce the ions observed for a given acquisition so that each measurement is dominated by the fragment ions of interest, reducing the contribution of background and contaminant ions (Supplemental Materials and Methods). In some cases, narrowing the mass window was not able to eliminate all contaminants, like for some of the aspartic acid mass spectral fragments in the Winter 2022 sample, as the aspartic acid abundances were so low (Table 1, Section 3.1) and the mass spectral peaks in some cases were less than one order of magnitude above the background. In the case of one aspartic acid fragment within the Winter 2022 sample (198 Da; Section 2.4), we were not confident that we would be able to perform a measurement free from artifacts introduced by contaminant ions. In general, we only included measurements of mass spectral fragments where contaminant ions made up <20% of the total ion count (TIC; Supplemental Materials and Methods), as suggested by Hofmann et al. in a prior study investigating the effects of contaminant ions on isotope ratios of other compounds in the same mixture (Hofmann et al., 2020). Hofmann et al. also demonstrated that resolutions of 60k mitigate the effects of contaminant ions (i.e., those that make up less than <20% of the TIC but that are still prominent in the mass window of interest) on the isotope ratios of the compound of interest; we used a resolution of 60k for measurements of lower-abundance mass spectral fragments. This was not an issue in our Spring 2021 specimen, as the amino acid abundances were higher in each replicate measurement, and thus those measurements were performed with resolutions of 120k. Measurements of more abundant fragments were performed with Automatic Gain Control (AGC) targets of $2 * 10^5$; less abundant fragments were performed with AGC targets of $5 * 10^4$ (Supplemental Materials and Methods; Table S3).

2.4. Isotope ratio measurement

Carbon isotope ratios of mass spectral fragments of α-alanine (m/z = 140.0323 Da; referred to as the 140 fragment), β-alanine (m/z = 126.0166 Da and referred to as the 126 fragment), and aspartic acid (unsubstituted masses of 113.0239 Da, 156.0272 Da, 198.0378 Da, referred to as the 113, 156 and 198 fragments) from Murchison were

Table 1
Concentrations and isotope ratios of the amino acids in this study compared to Chimiak et al., 2021s results. $\delta^{13}C$ values are reported in modeled PDB reference frame (mPDB*; see methods for details) ± propagated 1σ standard errors.

Sample	Amino Acid	Concentration (nmol/g)	L_{ee} (%)	Molecular Average $\delta^{13}C$	$\delta^{13}C_{amine}$ (‰, mPDB*, $\pm\sigma_{SE}$)	$\delta^{13}C_{acid\ 1}$ (‰, mPDB*, $\pm\sigma_{SE}$)	$\delta^{13}C_{averagemethyl/methylene}$ (‰, mPDB*, $\pm\sigma_{SE}$)	$\delta^{13}C_{acid\ 2}$ (‰, mPDB*, $\pm\sigma_{SE}$)
2021	L-α-alanine	8.2 ± 0.7§	0§					–
2021	D-α-alanine	8.3 ± 0.8§						
2021	β-alanine	16 ± 1§	–					–
2021	L-aspartic acid	1.7 ± 0.1§	28 ± 3§		−9 ± 10	13 ± 25	−32 ± 17	
2021	D-aspartic acid	0.95 ± 0.04§						
2022	L-α-alanine	2.97 ± 0.200	4.4 ± 7		+109 ± 25			–
2022	D-α-alanine	2.72 ± 0.202						
2022	β-alanine	9.128 ± 0.280	–		+33 ± 24			–
2022	L-aspartic acid	0.76 ± 0.017	23 ± 2		−14 ± 5			
2022	D-aspartic acid	0.48 ± 0.004						
Chimiak et al. (2021)	L-α-alanine	5.98 ± 1.03	6.0 ± 11	26 ± 3	+142 ± 20	−29 ± 10	−36 ± 20	–
Chimiak et al. (2021)	D-α-alanine	5.30 ± 0.88		25 ± 3				

§ Abundances for the Spring 2021 sample are based on data reported in (Glavin et al., 2020a). Prior molecular average $\delta^{13}C$ values of amino acids relevant to this study measured in hydrolyzed extracts of other specimens of Murchison are reported in Table S5 and discussed in Section 3.3.

measured relative to those of terrestrial standards (Supplemental Materials and Methods). With the Spring 2021 specimen, we measured the 113, 156, and 198 fragments of aspartic acid. With the Winter 2022 specimen, we measured the 156 fragment of aspartic acid, the 126 fragment of β-alanine and the 140 fragment of α-alanine.

Generally, to perform position-specific isotope ratio measurements on each sample, we required picomoles of the amino acid of interest for each replicate measurement of each fragment. To fully constrain each site of each amino acid, we needed to measure at least as many fragments are there were sites to constrain (to create a system of equations with an equal number of constraints and unknowns; Section 2.6; Supplemental Materials and Methods). This was not always possible with all amino acids in both samples, as we were sample-limited, and the abundance of amino acids was variable between the samples (Table 1). With these limitations in mind, we prioritized measuring sites that most directly tested synthesis hypotheses (i.e., the amine sites).

In some cases, we compare across specimens and across studies to constrain additional molecular sites. We used the Winter 2022 sample to constrain the amine site of aspartic acid, but we report position-specific carbon isotope values for the first carboxyl, and the methylene + second carboxyl carbon sites of aspartic acid based on measurements of the Spring 2021 sample (Sections 2.3 and 2.4). The Winter 2022 sample was also used to measure the mass spectral fragments constraining the amine sites of α-alanine and β-alanine (Sections 2.3 and 2.4). Measurements of the same fragment of aspartic acid (156 Da) for both the Spring 2021 and Winter 2022 sample were used as a proxy for heterogeneity between the samples, and used to justify comparison between the $\delta^{13}C$ values of aspartic acid fragments from the two specimens (discussed further in Sections 3 and 4). There was not enough Spring 2021 sample to measure fragments of α- or β-alanine. We only had enough sample to measure the amine site of α-alanine in the Winter 2022 site, so we use results from Chimiak et al., 2021 to constrain the methyl site of α-alanine (Section 3.2). We contextualize our results with past CSIA of Murchison amino acids (Section 3.3).

We compare sample fragment isotope ratios to those of amino acid standards with known molecular-average carbon isotopic composition. This comparison allows us to convert our measured isotope ratios into a standard reference frame analogous to the known international standard reference frame (i.e., VPDB for C) and report our data using standard carbon isotope delta notation, defined below (Eq. (1). We note that to perform this conversion from our "house standard" reference frame to the international standard, we must make an assumption that there is no intramolecular carbon isotope heterogeneity in our amino acid standards; we elaborate further on this assumption in Section 2.6.

We report fragment and position-specific isotope ratios in the common "delta" (δ) notation, calculated as the relative difference in isotope ratio between sample and standard, expressed in parts per thousand (per-mille; ‰):

$$\delta^{A}X = \left(\frac{{}^{A/a}R_{sample}}{{}^{A/a}R_{ref\ \ material}} - 1\right), \tag{1}$$

where A and a are the cardinal masses of the rare and common isotopes of interest, respectively, X is the formula of the isotope-substituted element in question, and R is the observed ratio of interest.

2.5. Solving for position-specific isotope values

The molecular structures of targeted fragments were determined by examining their exact masses and comparing potential molecular structures for each mass with predictions from spectral interpretation software (Mass Frontier, Thermo Scientific). Contributions from particular sites within the parent molecule were confirmed by measuring aspartic acid and β-alanine labeled (10% ^{13}C label) at each atom position (Supplemental Materials and Methods). We derived the following equations following a matrix math similar to what was described in Wilkes et al. for the computation of the position-specific carbon isotope values of serine (Wilkes et al., 2022). We note here that the following equations assume that delta values can be used as proxies for isotopic fractional abundances and therefore mix conservatively; while not precisely correct, this assumption leads to errors of up to 4‰ for the measured delta values which are within the measured analytical uncertainties of this study.

We identified one fragment (126) that allowed us to constrain the amine (C3) site of β-alanine (Fig. 2A):

$$\delta^{13}C_{C3} = 3{*}\delta^{13}C_{126} + \delta^{13}C_{VPDB,standard} \tag{2}$$

The other two sites of β-alanine can be constrained by measurement of the 139 Da fragment; we were not able to measure it due to prominent contaminants in the surrounding mass window, but include further description in the Supplementary Materials, as it would be a ripe target for future study (Supplemental Materials and Methods).

The fragmentation spectrum of α-alanine was confirmed by Chimiak et al. (2021), who demonstrated that the amine and methyl (C2 + C3) carbons can be constrained together by a measurement of the 140 Da fragment (Fig. 2B). In that study, they reported $\delta^{13}C_{VPDB}$ value for the methyl (C3) carbon site of −36 ± 20‰ for pristine Murchison. We had insufficient sample to complete a measurement of the other fragment necessary (m/z = 184.021) to constrain the methyl site alone. Thus, we use the value reported for the methyl (C3) carbon site of α-alanine by Chimiak et al. to compute a value for the amine (C2) site of alanine for our specimen as follows:

$$\delta^{13}C_{C2} = \left(\left(4{*}\delta^{13}C_{140}\right) - \left(\delta^{13}C_{amine} + \delta^{13}C_{VPDB,standard}\right)\right) + \delta^{13}C_{VPDB,standard} \tag{3}$$

This choice is supported by similarities in calculated $\delta^{13}C_{VPDB}$ values of the amine site of alanine from our study and Chimiak et al.'s (Section 3). A discussion of heterogeneity between Murchison specimens is included in Section 4.3.

We identified three fragments of aspartic acid (113, 156, and 198) that permitted us to calculate position-specific values for the first carboxyl (C1) and amine (C2) sites of aspartic acid, and the methylene and second carboxyl (C3 + C4) sites together (Fig. 2C):

$$\delta^{13}C_{C1} = 5{*}\delta^{13}C_{113} - 6{*}\delta^{13}C_{198} + \delta^{13}C_{VPDB,standard} \tag{4}$$

$$\delta^{13}C_{C2} = 4{*}\delta^{13}C_{156} + \delta^{13}C_{VPDB,standard} \tag{5}$$

$$\delta^{13}C_{C3+C4} = 6{*}\delta^{13}C_{198} - 4{*}\delta^{13}C_{156} + \delta^{13}C_{VPDB,standard} \tag{6}$$

Like β-alanine, the four sites could be fully constrained via measurement of the 138 Da fragment, but there were too many contaminants within the surrounding mass window to provide a confident measurement (Supplemental Materials and Methods).

The matrices and equations used for these position-specific computations for all three compounds are depicted in Figs. 2 and S2. For each conversion, we assume that exogenous derivative atoms have identical isotopic compositions for both the sample and standard. This is a reasonable assumption because the sample and standard are derivatized at the same time under identical conditions and this derivative is known to fractionate C in a reproducible manner (Corr et al., 2007; Silverman et al., 2021).

Errors for isotope ratio measurements are reported as standard errors across replicate acquisitions (σ_{SE}):

$$\sigma_{SE} = \frac{\sigma}{\sqrt{n}}, \tag{7}$$

where σ is the standard deviation of the average isotope ratios for the set of replicate acquisitions, and n is the number of acquisitions. For position-specific isotope ratio measurements, σ_{SE} of the fragment delta values were propagated in quadrature following the fragment to position-specific matrix conversions (Supplemental Materials and

Methods). Both σ and σ_{SE} are reported in ‰.

2.6. Conversion to modeled VPDB (mPDB*) space and relevant assumptions

It is important to contextualize our results within the already-established framework of the stable isotope geochemistry of carbon. As such, we converted position-specific $\delta^{13}C$ values measured within our house standard reference frame into the more widely used 'primary standard' isotope scales (e.g., VPDB; Brand et al., 2014), which we refer to as "modeled VPDB" (mPDB*), as demonstrated by Eq. (6). To perform this conversion from our house standard reference frame to mPDB* reference frame, we added the measured compound-specific $\delta^{13}C_{VPDB}$ value of each standard as measured by the EA to our measured fragment delta values in the house standard reference frame. Similar to the assumption made for Equations 2–6 presented above, our conversion to mPDB* reference frame assumes conservative mixing of delta values.

Our mPBD* reference frame also incorporates an assumption that there is no intramolecular variation in carbon isotopic composition across the standard. This is not true for previously studied terrestrial amino acids; for instance, the first PSIA study by Abelson and Hoering demonstrated via ninhydrin reaction of amino acids extracted from *Chlorella pyrenoidosa* that the $\delta^{13}C_{VPDB}$ values of the carboxyl sites of α-alanine and aspartic acid are higher – $\delta^{13}C_{VPDB}$ = 11.9‰ and 8.7‰, respectively – than the average of the other remaining sites – $\delta^{13}C_{VPDB}$ = −14.8‰ and −15.7‰, respectively (Abelson and Hoering, 1961). Intramolecular variations in carbon isotopic composition across commercially synthesized standards are even smaller (i.e., 10–15‰, constrained by via ninhydrin reaction; Chimiak and Eiler, 2022), and within the errors that we report for each site. As such, we do not characterize these standard site-level differences here or incorporate them into our calculation of site-specific isotope ratios, but future studies could further improve the presentation of their isotope ratios on the international standard scale by adding additional measurements of the standard (based on EA-IRMS or nuclear magnetic resonance (NMR) constraints (e.g., Gilbert et al., 2009).

3. Results

3.1. Amino acid abundances

Abundances of L- and D-α-alanine from the Spring 2021 sample were 8.2 ± 0.7 and 8.3 ± 0.8 nmol/g, respectively. Abundances of L- and D-α-alanine from the Winter 2022 sample were 2.97 ± 0.200 and 2.72 ± 0.202 nmol/g, respectively. β-alanine abundances in the Spring 2021 and Winter 2022 samples were 16 ± 1 and 9.128 ± 0.280 nmol/g, respectively. Abundances of L- and D-α-aspartic acid from the Spring 2021 sample were 1.7 ± 0.1 nmol/g and 0.95 ± 0.04, respectively. Abundances of L- and D-α-aspartic acid from the Winter 2022 sample were 0.76 ± 0.017 nmol/g and 0.48 ± 0.004, respectively. Amino acid abundances for the Spring 2021 sample were reported originally in Glavin et al. (2020a). Overall, abundances in the Winter 2022 sample were half or less of the abundance of the same amino acids measured in the Spring 2021 sample.

α-Alanine enantiomers in both the Spring 2021 and Winter 2022 samples have been observed in near-racemic proportions (L_{ee} = 0) within error (Table 1) indicating that these samples are minimally contaminated (Friedrich et al., 2019; Glavin et al., 2020a; Chimiak et al., 2021). The L_{ee} of aspartic acid for these chips is consistent with a previous report from the same stone (Glavin et al., 2020a), and has been proposed to be endogenous to the meteorite, though this interpretation could not be confirmed in that study by isotopic analysis of each enantiomer due to low abundances of aspartic acid within the measured sample. Nevertheless, the similarity in the $\delta^{13}C$ values of the 156 Da fragment ion of aspartic acid in both specimens examined in this study provides additional support that the amino acids in the two different specimens of Murchison are similar in origin and are endogenous to the sample; i.e., it is unlikely that the same amino acids from two distinct specimens of the same meteorite experienced equal amounts of contamination resulting in the same position-specific $\delta^{13}C$ values (Section 3.2).

3.2. Position-specific isotope values of Murchison amino acids

Fragment ion $\delta^{13}C$ values (Table S1) were converted into position-specific $\delta^{13}C$ values (Table S2), which were converted from the reference frame of a standard with known isotopic composition into our mPDB* reference frame (Figs. 2 & 3, Table 1, Table S2). Our measurements constrained the amine carbon $\delta^{13}C$ values for α- and β-alanine as $\delta^{13}C_{mPDB*}$ = +109 ± 21‰ and + 33 ± 24‰, respectively (Fig. 3). These values are ^{13}C-enriched relative to any previously studied terrestrial amino acid. In contrast, the aspartic acid extract of the same specimen yielded an amine site $\delta^{13}C_{mPDB*}$ = −14 ± 5‰ (Fig. 3). The $\delta^{13}C$ value of the amine carbon of aspartic acid was equal within error to that of the terrestrial standard (Fig. 3).

Our measurement of the $\delta^{13}C$ of α-alanine's amine site is equal within error to the value previously measured for a different sample of Murchison (+142 ± 20‰; Fig. 3; Chimiak et al., 2021), suggesting that we can directly compare data generated in these two studies, and specifically supports our use of the $\delta^{13}C$ value of the methyl site of α-alanine reported by Chimiak et al. ($\delta^{13}C_{VPDB}$ = −36 ± 20‰) to constrain the site-specific values of our measured α-alanine.

$\delta^{13}C$ values of the amine carbons of aspartic acid extracted from Spring 2021 and Winter 2022 specimens were within error of each other, which suggests some consistency between samples and supports our choice to use the measurements of the Spring 2021 sample to constrain aspartic acid's full position-specific carbon isotopic composition. Measurements of aspartic acid from the Spring 2021 specimen demonstrate that the average $\delta^{13}C$ of the methylene and second carboxyl carbon sites (not observed separately in this specimen) is $\delta^{13}C_{mPDB*}$ = −32 ± 17 – lower than (but within 2 standard errors of) the terrestrial standard's – while the $\delta^{13}C$ of the first carboxyl carbon site is higher than the standard's ($\delta^{13}C_{mPDB*}$ = 13 ± 25; Table 1; Fig. 3).

4. Discussion

Our measured $\delta^{13}C$ value of α-alanine's amine site, averaged with the carboxyl and methyl sites reported in Chimiak et al., 2021 ($\delta^{13}C_{VPDB}$ = −28.7‰ and −36.3‰, respectively) reproduces a molecular-average $\delta^{13}C$ value consistent within error with those measured in past CSIA of Murchison alanine (+25–52‰; Table S5; Engel et al., 1990; Pizzarello et al., 2004; Elsila et al., 2012; Glavin et al., 2020b; Chimiak et al., 2021). Our measured $\delta^{13}C$ value of β-alanine's amine site would be consistent with several measurements of the molecular-average $\delta^{13}C$ from prior CSIA of β-alanine ($\delta^{13}C_{VPDB}$ = +5 to +10‰; (Pizzarello et al., 2004, 2006; Glavin et al., 2020a) if we assumed the isotopic composition of the combined methylene and carboxyl sites from β-alanine are comparable to that of the terrestrial standard ($\delta^{13}C_{VPDB}$ ~ −30‰), as is the case for the non-amine carbons in Chimiak et al.'s study of α-alanine (2021), as well as our methylene and second carboxylic acid carbons in the aspartic acid measured in the Spring 2021 sample. Our position-specific $\delta^{13}C$ values of aspartic acid, averaged across all four sites, are consistent within error with the molecular-average $\delta^{13}C$ of this same compound from Murchison ($\delta^{13}C_{VPDB}$ = +4‰), determined previously by CSIA (Table S5; Pizzarello et al., 1991). A prior CSIA by Pizzarello and others of the D- and L- enantiomers of aspartic acid reported $\delta^{13}C_{VPDB}$ values of −25.2 and −6.2‰, respectively, but they acknowledged lower $\delta^{13}C$ values for the L-enantiomers could be caused by terrestrial contamination (Pizzarello et al., 2004), which as we have already noted, we expect to be minimal or similar for our two measured Murchison specimens.

Our results suggest that α-alanine and β-alanine both formed from

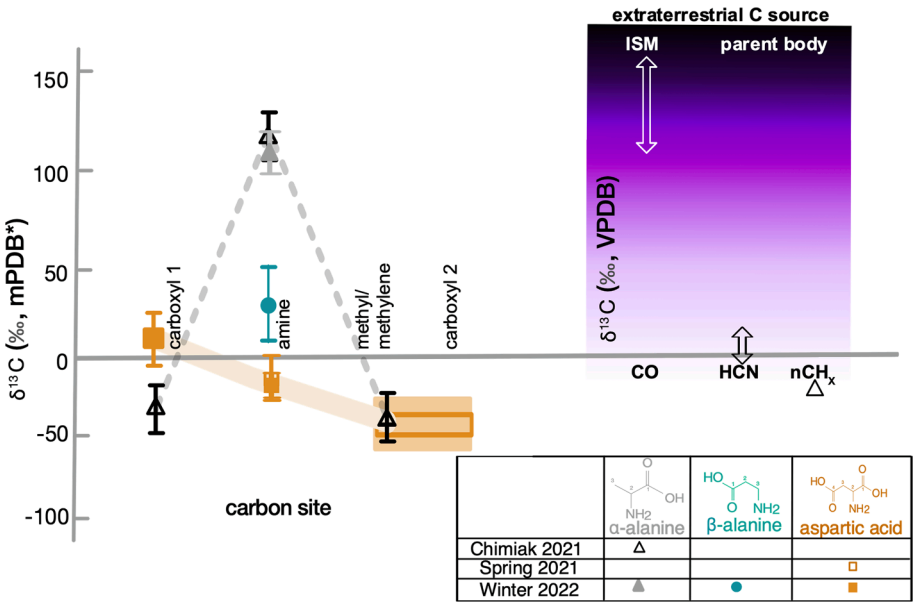

Fig. 3. Position-specific carbon isotope values. $\delta^{13}C$ values of carbon positions for α-alanine (this study = grey triangle; (Chimiak et al., 2021) = open black triangle), β-alanine (teal circle) and aspartic acid (orange squares; open = Spring 2021, closed = Winter 2022) reported within our mPDB* reference frame. Error bars are $2\sigma_{SE}$. Key is inset within the table in the lower right. $\delta^{13}C$ values of different carbon sources within the ISM and on the meteorite parent body (Table S6) are plotted alongside for comparison, which have a range of isotopic compositions that could contribute to the amino acid's during synthesis. (For interpretation of the references to colour in this figure legend, the reader is referred to the web version of this article.)

^{13}C-enriched precursors, plausibly from the ISM, though with a significant difference in the final resulting $\delta^{13}C$ that potentially reflects distinct reaction pathways linking those precursors to final products. In contrast, aspartic acid appears to have formed entirely from precursors originating from relatively ^{13}C-depleted carbon sources (i.e., broadly resembling average meteoritic and terrestrial organic carbon); this implies that aspartic acid likely formed via a different reaction mechanism from both α and β-alanine, and possibly formed from precursors derived from the most common and abundant carbon components of the meteorite parent body. The similarity between the values of the methylene and second carboxylic acid carbons in aspartic acid and the methylene carbons in α-alanine further suggests the existence of shared carbon "pools" from which some carbons of different precursors derive. Indeed, prior work has suggested that carbon in meteoritic organic molecules are inherited from three potential sources: a ^{13}C-enriched CO pool from the ISM vs. relatively ^{13}C-depleted pools from HCN and nCH_x, possibly in the ISM and certainly on the meteorite parent body (Fig. 3; Elsila et al., 2012).

Characterization of the isotopic compositions of carbon "pools" from which amino acids formed can be combined with known mechanisms of abiotic amino acid synthesis and isotope effects (IEs) imparted at each elementary reaction step to support or reject hypotheses regarding potential formation mechanisms. Reaction rates of elementary steps of irreversible reactions may differ between isotopic forms of reactants (kinetic isotope effects, or KIEs). Reversible exchange between reactants and products can result in equilibrium differences in isotopic content between the two (equilibrium isotope effects; EIEs). In both cases, IEs are quantified by the variable, ε, expressed as a difference in isotope ratio between reactant and product:

$$\varepsilon^{i}_{j-k} = 1000^{*}\left(\alpha^{i}_{j-k} - 1\right), \tag{8}$$

where α^{i}_{j-k} is the ratio of isotope ratios of the product and reactant, respectively, and the ε variable converts this α value into units of ‰. Negative ε^{i}_{j-k} values are "normal" isotope effects where the products are less heavy-isotope enriched than the reactants. These isotopic fractionations associated with reactions are specific to the reaction type and imprinted differently on different atomic sites of the product; thus, PSIA can help identify reaction types and therefore improve on constraints available from conventional isotope analyses.

4.1. *Extraterrestrial Strecker synthesis of ^{13}C-enriched α-alanine*

Both our study and the prior study by Chimiak et al. (2021) measured a $\delta^{13}C$ value of α-alanine's amine carbon that is highly ^{13}C-enriched compared to terrestrial organic carbon and molecular-average values of most C-rich compounds found in the carbonaceous chondrites. Chimiak et al. demonstrated that the PSIA of α-alanine from Murchison supports the hypothesis that it formed through Strecker-Cyanohydrin synthesis, whereby a distinctively ^{13}C-enriched amine carbon site was inherited from a ^{13}C-enriched carbonyl group of an aldehyde precursor (originally from interstellar CO), whereas the less ^{13}C-rich carboxyl and methyl sites of α -alanine were inherited from HCN and the CH_n moieties of aldehyde precursors, respectively.

We apply Chimiak et al.'s model (along with experimental data from Chimiak et al., 2022) to interpret our new measurement of the $\delta^{13}C$ value of the amine carbon of α-alanine; this approach lets us back-calculate the original $\delta^{13}C$ value of the precursor aldehyde molecule, applying the EIE (ε) for the addition of CN (average $\varepsilon = -20$‰; depicted in Fig. 4A and originally reported in Chimiak et al., 2021, 2022) to solve for a $\delta^{13}C$ value of ~130‰ of the precursor carbon – the carbonyl site of reactant aldehyde. This result is consistent with prior studies that have measured and modeled higher $\delta^{13}C$ values of CO in the ISM ($\delta^{13}C$ = 110–160‰; Lyons et al., 2018; Chimiak et al., 2021). We used this value as the starting point for ^{13}C-enriched amine sites for the rest of our modeled Strecker-related reactions (Fig. 4A). Hydrolysis also introduces an isotope effect on the reacting carbon ($\varepsilon = -10$‰ on C1 of α-alanine; Fig. 4A), but it is within the range of our analytical error and the error reported by Chimiak et al (2021) on the position-specific carbon isotope value of carboxyl carbon. The other reaction steps involved in Strecker synthesis of α-alanine do not have measurable IEs (Chimiak et al., 2022).

A Strecker synthesis formation mechanism for α-alanine is supported by past CSIA (Elsila et al., 2012; Aponte et al., 2017; Chimiak et al., 2021); for instance, the observation that the $\delta^{13}C$ value of α-amino acids decreases with increasing number of carbon atoms (Sephton, 2002), which has been interpreted to reflect a dilution of a ^{13}C-enriched aldehyde precursor with added HCN/nCH_x-derived carbons (Elsila et al., 2012; Chimiak et al., 2021; Chimiak and Eiler, 2022). FTT synthesis is disfavored as a path to forming these compounds, as it would not create such distinctive differences in intramolecular isotopic composition, and is incapable of explaining the pattern of intermolecular differences in molecule average C isotope composition documented in many past studies (Chimiak et al., 2021). More work is necessary to understand

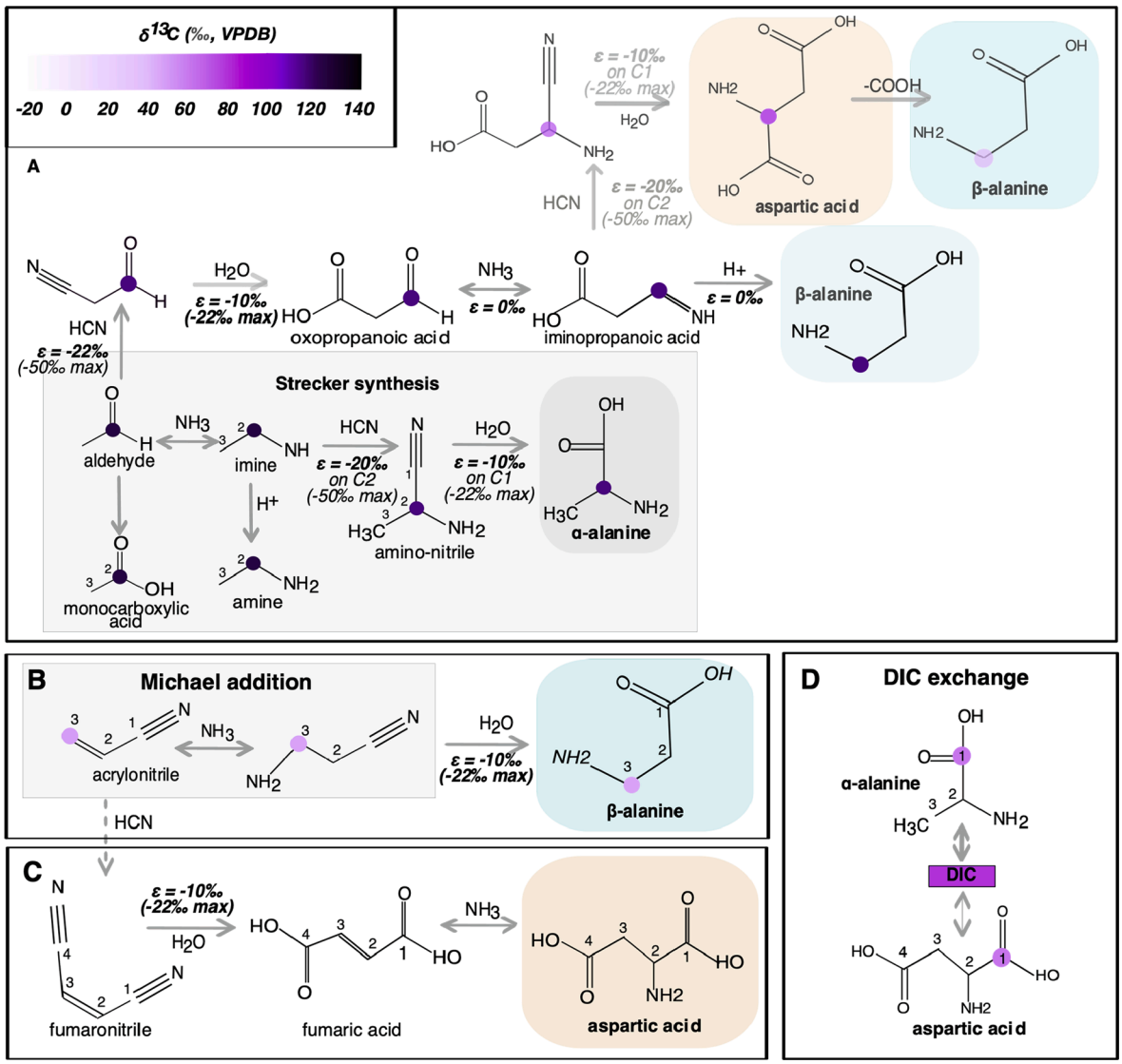

Fig. 4. Potential extraterrestrial amino acid synthesis pathways, and ^{13}C enrichments of their amine sites. (A) Extraterrestrial α-amino acids, including α-alanine, are thought to be synthesized via Strecker synthesis (grey box; (Elsila et al., 2012; Chimiak et al., 2021)), which inherits an ^{13}C-enriched carbon from interstellar medium CO in its amine carbon site (value derived from the $\delta^{13}C$ value of α-alanine's amine carbon). There are potential pathways to form β-alanine and aspartic acid through related reactions, but we rule out synthesis through these pathways from the same precursors of α-alanine and thus those pathways are shown in grey. (B) Michael addition of a nucleophile to an unsaturated carbonyl compound (acrylonitrile) is a common hypothesis for the formation of β-alanine (Burton et al., 2012; Elsila et al., 2012). For this pathway to be consistent with the $\delta^{13}C$ value we measured in β-alanine's amine site, the acrylonitrile precursor would need to be ^{13}C-enriched in its terminal carbon (Chimiak and Eiler, 2022). (C) Aspartic acid can also be synthesized via either amination of an unsaturated dicarboxylic acid or reductive amination of α-keto acid, likely via a fumaronitrile precursor. If all these carbons originated from the ^{13}C-depleted carbon pool on the meteorite parent body, the carbon isotope values of the amine site should not be noticeably higher than the values of other sites, as we observe in our results. It is possible that the fumaronitrile precursor may form from acrylonitrile (dotted arrow), but could not have the same enrichment as observed in β-alanine to be consistent with the value we measured for aspartic acid's amine site. (D) Carboxyl carbons could exchange with the carbonate in the host rock and become more ^{13}C-enriched.

isotopic fractionations related to amino acid formation via irradiation of methanol-containing ices, so our data and model arguments should not be construed as disproof of this alternative hypothesis.

4.2. *Additional pathways required for synthesis of β-alanine and aspartic acid*

Understanding the potential pathways to forming β-alanine and aspartic acid is more challenging, as there are diverse hypotheses as to how synthesis of these amino acids may occur and prior compound-specific carbon isotope data do not clearly discriminate among these possibilities. Three possible ways to synthesize β-alanine are established in the literature: reductive amination of an oxopropanoic acid intermediate that was itself formed via Strecker synthesis (Fig. 4A); decarboxylation of aspartic acid (Fig. 4A); and Michael addition of an unsaturated carbonyl (i.e., acrylonitrile) which is then aminated and hydrolyzed to form β-alanine (Fig. 4B; Peltzer et al., 1984; Burton et al., 2012; Elsila et al., 2012).

The $\delta^{13}C_{mPDB*}$ value of β-alanine's amine carbon is enriched, but less enriched than that of α-alanine's amine carbon for the specimens measured in this study. We rule out synthesis exclusively by a Strecker synthesis mechanism (i.e., reductive amination of an oxopropanoic acid intermediate, where the amine carbon is inherited from interstellar ^{13}C-enriched CO; Fig. 4A), as the same precursors that made the α-alanine measured here could not have synthesized a β-alanine that is consistent with our PSIA: β-alanine would have to be much more enriched.

Our findings are also inconsistent with β-alanine within Murchison forming exclusively via decarboxylation of aspartic acid, or at least

based on the PSIA of aspartic acid measured in this study. Decarboxylation imparts an IE (ε = 2–40‰, depending on whether it is catalyzed or uncatalyzed; (O'Leary and Yapp, 1978; Lewis et al., 1993)), so if Murchison β-alanine formed this way from decarboxylation of Murchison aspartic acid, the $\delta^{13}C$ value of β-alanine's amine carbon should be similar to or lower than that of the aspartic acid it formed from, which is inconsistent with our results.

Thus, we propose that the β-alanine measured in this study was synthesized via Michael addition of a nucleophile to an unsaturated carbonyl compound (e.g., acrylonitrile; Fig. 4B). The expected intramolecular isotopic composition of an acrylonitrile is debated in the literature, ranging from no expected intramolecular carbon heterogeneities (Elsila et al., 2012) to the formation of a nitrile where the terminal carbon could inherit a ^{13}C enrichment from interstellar CO (Fig. 4B; (Chimiak and Eiler, 2022)). It is also possible that β-alanine's $\delta^{13}C$ value could represent a combination of synthesis processes, where β-alanine with a ^{13}C-enriched-amine site, produced through some combination of reactions in Fig. 4A, is diluted by formation of β-alanine through processes resembling Michael addition (Fig. 4B) or aspartic acid decarboxylation (Fig. 4C) with smaller isotope effects. Additional position-specific isotope measurements of β- amino acids with longer carbon chains (e.g., β-amino n-butyric acid) could help to further narrow down the most plausible synthesis mechanisms for this class of molecules.

Aspartic acid's lower $\delta^{13}C$ values at all measured carbon positions, particularly compared to the ^{13}C-rich amine carbons of α- and β-alanine, suggest that a distinct mechanism (or combination of mechanisms) must be responsible for its formation. Proposed mechanisms to form aspartic acid abiotically include: Strecker synthesis via an oxopropanoic acid intermediate (Fig. 4A), or synthesis via either amination of an unsaturated dicarboxylic acid or reductive amination of α-keto acid, likely through a fumaronitrile precursor (Fig. 4C; (Pizzarello et al., 2006; Burton et al., 2012)).

It is possible that the aspartic acid measured in our specimen was formed via the Strecker pathway, but to be consistent with our measurements either the KIEs from two or more reaction steps would have to be maximally expressed, or the aspartic acid would need to be synthesized from aldehyde precursors with lower $\delta^{13}C$ values of the carbonyl site than the precursors responsible for synthesis of α-alanine (Simkus et al., 2019b). Thus, aspartic acid could not have formed by Strecker synthesis as part of the same reaction network with the same precursors that formed α- and β-alanine, but could have formed by Strecker synthesis from a separate set of precursors (perhaps in a different environment).

Alternatively, aspartic acid's ^{13}C-depleted amine, methylene and second carboxyl carbons are consistent with synthesis via a fumaronitrile precursor in the meteorite parent body, from the same HCN and $nCOH_x$ precursors that have been previously called on to explain synthesis of amino acids (Chimiak et al., 2021, and preceding sections of this paper). Precursors for such reactions that could have been present in the meteorite parent body include unsaturated dicarboxylic acids, which have been identified in Murchison (e.g., fumaric acid; Sephton, 2002). Prior studies have performed CSIA of dicarboxylic acids (Cronin et al., 1993; Pizzarello et al., 2001), finding $\delta^{13}C$ values ranging from 28 to −6‰, similar to the range of measured $\delta^{13}C$ values for aspartic acid (Table S5). Average IEs associated with converting ^{13}C-depleted fumaronitrile precursors (Table S6) into aspartic acid would be −22‰ to each reacting carbon for the addition of water (Fig. 4C), and thus result in aspartic acid without intramolecular ^{13}C enrichments (at the scale resolved in this study). Interestingly, synthesis via the fumaronitrile precursor has been posited as a plausible pathway to synthesize organics on early Earth via a cyanosulfidic protometabolism under subtly alkaline conditions (Patel et al., 2015).

4.3. Heterogeneity in the abundances and isotopic compositions of meteoritic organics

Organic chemical and stable isotopic heterogeneities among carbonaceous chondrites have long been documented. Amino acid molecular average $\delta^{13}C$ values vary depending on the specimen analyzed (Glavin et al., 2010). This isotopic variation may reflect spatial or temporal variations in isotopic compositions of precursors of organic compounds (e.g., $\delta^{13}C$ of interstellar CO varies from 110 to 160‰; $\delta^{13}C$ of aldehydes and ketones extracted from Murchison range from −10 to 66‰; Table S6; Lyons et al., 2018; Simkus et al., 2019b; Chimiak et al., 2021), or a combination of synthesis processes, as discussed here.

Both our study and prior studies have highlighted variable amino acid abundances within distinct specimens of the same meteorite (Glavin et al., 2010 and data herein, Section 1, Table 1). These variations in abundances could be driven by primary (i.e., formation) or secondary (i.e., redistribution and alteration) processes. Prior research has demonstrated that aqueous alteration can affect the abundance of amino acids, linking β-alanine abundance with degree of alteration, suggesting some amino acid formation mechanisms may be more productive with more abundant water (Botta et al., 2007). Likewise, aqueous alteration can alter the isotopic compositions of meteoritic amino acids, as isotopic variations can arise from differences in extents of isotopic exchange between the studied organic compounds and other parent body reservoirs (i.e., carbonate during aqueous alteration; Pietrucci et al., 2018). Different degrees of carbonate exchange in the carboxyl site of amino acids may be responsible for the heterogeneity in prior molecular average $\delta^{13}C$ measurements (Table S5) and to the values presented in our study. For instance, aspartic acid's first carboxyl site has a higher $\delta^{13}C$ value than the equivalent site in the terrestrial standards, which could be driven by exchange with dissolved inorganic carbon in parent body waters; carbonates in the aqueous alteration assemblage of the Murchison meteorite that have been demonstrated to be ^{13}C-enriched, reaching a maximum $\delta^{13}C_{VPDB}$ of 80‰ (Alexander et al., 2015; Telus et al., 2019). Indeed, carboxyl-carbonate exchange was suggested by Chimiak et al., 2021 as one possible explanation of differences between the $\delta^{13}C$ value of the C_1 carboxylic acid carbons of their method development and analytical samples. It is notable that the $\delta^{13}C$ values measured here and by Chimiak et al., 2021 for amino acid carboxyl sites have a range of values, but that none reach the maximum observed for carbonate grains in CCs, suggesting that even though exchange may be occurring, amino acid carboxyl sites do not reach full equilibrium with the dissolved inorganic carbon of parent body fluid.

Finally, sample preparation procedures may bias which amino acids are released from the meteorite sample via acid hydrolysis. Acid hydrolysis frees amino acids otherwise bound within larger polymers, and is used routinely in the preparation of meteoritic amino acids for analysis (Elsila et al., 2012; Simkus et al., 2019a). The starting materials for the hydrolyzed amino acids released from meteorites remain mostly unknown, and it is possible that the production of amino acids from unknown precursors could have an effect on the isotopic composition of the measured amino acids (Simkus et al., 2019b). However, one prior study demonstrated no appreciable difference in the compound-specific carbon isotopes of amino acids within two —CH_3 carbonaceous chondrites measured in the unhydrolyzed versus hydrolyzed extracts (Burton et al., 2013). It is also compelling that known isotope effects for each proposed reaction step in our posited mechanisms (Fig. 4) can connect our measured position-specific isotope effects with previously measured isotope values of potential reactant molecules (Table S6).

5. Conclusions

Amino acids on meteorites are formed from precursors including interstellar components, through a heterogeneous and complex reaction network combining Strecker synthesis, Michael addition, and a fumaronitrile-based process that resembles posited mechanisms of

prebiotic chemistry on Earth. Our observations are consistent with a scenario in which α-alanine formed entirely through Strecker synthesis, drawing on aldehyde precursors with a ^{13}C-enriched carbonyl site (presumably inherited from CO in the ISM), and ^{13}C-depleted non-carbonyl sites as well as ^{13}C-depleted HCN. In contrast, β-alanine could have formed via Michael addition drawing on both ^{13}C-enriched CO-derived and ^{13}C-depleted HCN precursors. Aspartic acid is most consistent with synthesis via a fumaronitrile precursor with no ^{13}C-enriched position-specific isotope values and thus likely derived from ^{13}C-depleted HCN. This network also calls on reaction mechanisms that require liquid water and neutral-to-mildly alkaline conditions, and thus could potentially occur (and compete with one another and other reactions) contemporaneously on the meteorite parent body.

This study has addressed one of several questions raised by the hypothesis in Chimiak et al. (2021) and Chimiak and Eiler (2022), i.e., that a broad spectrum of soluble organics in the several of the carbonaceous chondrites share a synthetic history as components of a Strecker-based reaction network. Future studies should further test, modify and/or extend this hypothesis through additional PSIA of other meteoritic organics; we believe such work will make progress most quickly by focusing on branched amino acids, amines, and hydroxy acids, as the Chimiak et al. hypothesis explains their molecular average isotopic compositions through mechanisms that are predicted to leave specific, high-amplitude site-specific isotopic signatures. Understanding secondary alteration (pre- and post-fall) and its effects on contamination and alteration of intramolecular isotopic composition of meteoritic amino acids would also be invaluable to progressing this work. Development of methods for an improved understanding of extraterrestrial organic synthesis is more important now than ever; this study and others like it will be central in understanding the carbon isotopic composition, source and synthesis of any organics found through Mars Sample Return, NASA's OSIRIS Perseverance, OSIRIS-REx mission, JAXA's Hayabusa2 and MMX missions, and future sample return missions from organic-rich objects to elucidate the astrochemical and potential biochemical synthetic pathways beyond Earth.

Research data

Research data has been supplied via a repository: https://doi.org/10.5281/zenodo.7549008.

CRediT authorship contribution statement

Sarah S. Zeichner: Methodology, Validation, Formal analysis, Investigation, Data curation, Software, Visualization, Supervision, Project administration. **Laura Chimiak:** Methodology, Validation, Formal analysis, Investigation. **Jamie E. Elsila:** Methodology, Validation, Formal analysis, Writing – review & editing. **Alex L. Sessions:** Conceptualization, Methodology, Writing – review & editing. **Jason P. Dworkin:** Conceptualization, Formal analysis, Writing – review & editing. **José C. Aponte:** Conceptualization, Formal analysis, Writing – review & editing. **John M. Eiler:** Conceptualization, Methodology, Supervision, Resources, Funding acquisition.

Declaration of Competing Interest

The authors declare that they have no known competing financial interests or personal relationships that could have appeared to influence the work reported in this paper.

Data availability

MurchisonAminoAcids (Original data) (Github).

Acknowledgement and funding sources

We thank Elise Wilkes, Elliott Mueller, Tim Csernica, Surjyendu Bhattacharjee, Guannan Dong, Amy Hofmann, and Kate Freeman for feedback and discussion on topics ranging from GC-Orbitrap methodology to data processing. Peter Martin, Max Lloyd, Andreas Hilkert, Kostya Ayzikov, and Caj Neubauer provided invaluable contributions to the development of Orbitrap data analysis software. These experiments would have been impossible without Nami Kitchen's and Fenfang Wu's unwavering support with instrumentation. We thank Dr. Robert Minard and Dr. Clifford N. Matthews' research group at the University of Illinois at Chicago for providing the Murchison meteorite. We are grateful for funding support from the Planetary Science Division funding through the Goddard Center for Astrobiology and the Fundamental Laboratory Research (FLaRe) work package, by the DOE BES program (to J.M.E.), and by the Simons Foundation (SCOL award 302497 to J.P.D. and award 626103 to J.M.E.). SSZ was funded by the National Science Foundation Graduate Research Fellowship.

Appendix A. Supplementary material

The supplementary material for this paper includes additional details of the materials and methods used in this study, including descriptions of amino acid standards, Orbitrap mass-spectrometry, position-specific isotope ratio analysis, data processing, and error propagation. There is also a section within the "data analysis" section that describes how one could constrain every molecular position of each amino acid characterized within this study, using the same methods. Finally, the supplement includes two additional figures and six additional tables that provide additional raw data, methodological context, and collation of prior relevant data from other studies. Supplementary material to this article can be found online at https://doi.org/10.1016/j.gca.2023.06.010.

References

Abelson, P.H., Hoering, T., 1961. Carbon isotope fractionation of amino acids by photosynthetic organisms. Proc. Natl. Acad. Sci. 47, 623–632.
Alexander, C.M.O.D., Bowden, R., Fogel, M.L., Howard, K.T., 2015. Carbonate abundances and isotopic compositions in chondrites. Meteorit. Planet. Sci. 50, 810–833.
Aponte, J.C., Elsila, J.E., Glavin, D.P., Milam, S.N., Charnley, S.B., Dworkin, J.P., 2017. Pathways to meteoritic glycine and methylamine. ACS Earth Space Chem. 1, 3–13.
Bernstein, M.P., Dworkin, J.P., Sandford, S.A., Cooper, G.W., Allamandola, L.J., 2002. Racemic amino acids from the ultraviolet photolysis of interstellar ice analogues. Nature 416, 401–403.
Botta, O., Bada, J.L., 2002. Extraterrestrial organic compounds in meteorites. Surv. Geophys. 23, 411–467.
Botta, O., Martins, Z., Ehrenfreund, P., 2007. Amino acids in Antarctic CM1 meteorites and their relationship to other carbonaceous chondrites. Meteorit. Planet. Sci. 42, 81–92.
Brand, W.A., Coplen, T.B., Vogl, J., Rosner, M., Prohaska, T., 2014. Assessment of international reference materials for isotope-ratio analysis (IUPAC technical report). Pure Appl. Chem. 86, 425–467.
Burton, A.S., Stern, J.C., Elsila, J.E., Glavin, D.P., Dworkin, J.P., 2012. Understanding prebiotic chemistry through the analysis of extraterrestrial amino acids and nucleobases in meteorites. Chem. Soc. Rev. 41, 5459–5472.
Burton, A.S., Elsila, J.E., Hein, J.E., Glavin, D.P., Dworkin, J.P., 2013. Extraterrestrial amino acids identified in metal-rich CH and CB carbonaceous chondrites from Antarctica. Meteorit. Planet. Sci. 48, 390–402.
Cerling, T.E., Harris, J.M., MacFadden, B.J., Leakey, M.G., Quade, J., Eisenmann, V., Ehleringer, J.R., 1997. Global vegetation change through the Miocene/Pliocene boundary. Nature 389, 153–158.
Charnley, S.B., Ehrenfreund, P., Millar, T.J., Boogert, A.C.A., Markwick, A.J., Butner, H. M., Ruiterkamp, R., Rodgers, S.D., 2004. Observational tests for grain chemistry: Posterior isotopic labelling. MNRAS 347, 157–162.
Chimiak, L., Eiler, J., 2022. Prebiotic Synthesis on Meteorite Parent Bodies: Insights from Hydrogen and Carbon Isotope Models. ChemRxiv, Cambridge.
Chimiak, L., Elsila, J.E., Dallas, B., Dworkin, J.P., Aponte, J.C., Sessions, A.L., Eiler, J.M., 2021. Carbon isotope evidence for the substrates and mechanisms of prebiotic synthesis in the early solar system. Geochim. Cosmochim. Acta 292, 188–202.
Chimiak, L., Eiler, J., Sessions, A., Blumenfeld, C., Klatte, M., Stoltz, B.M., 2022. Isotope effects at the origin of life: Fingerprints of the Strecker synthesis. Geochim. Cosmochim. Acta 321, 78–98.

Cordiner, M.A., Palmer, M.Y., Charnley, S.B., Paganini, L., Villanueva, G., 2019. ALMA autocorrelation spectroscopy of comets: The HCN / $H^{13}CN$ ratio in C/2012 S1 (ISON). Astrophys. J. Lett. 870, L26.
Corr, L.T., Berstan, R., Evershed, R.P., 2007. Optimisation of derivatisation procedures for the determination of $\delta^{13}C$ values of amino acids by gas chromatography/combustion/isotope ratio mass spectrometry. Rapid Commun. Mass Spectrom. 21, 3759–3771.
Cronin, J.R., Pizzarello, S., Epstein, S., Krishnamurthy, R.V., 1993. Molecular and isotopic analyses of the hydroxy acids, dicarboxylic acids, and hydroxydicarboxylic acids of the Murchison meteorite. Geochim. Cosmochim. Acta 57, 4745–4752.
DeNiro, M.J., Epstein, S., 1977. Mechanism of carbon isotope fractionation associated with lipid synthesis. Science 197, 261–263.
Eiler, J., Cesar, J., Chimiak, L., Dallass, B., Grice, K., Griep-Raming, J., Juchelka, D., Kitchen, N., Lloyd, M.K., Makarov, A., Robins, R., Schwieters, J., 2017. Analysis of molecular isotopic structures at high precision and accuracy. Int. J. Mass Spectrom. 422, 126–142.
Elsila, J.E., Charnley, S.B., Burton, A.S., Glavin, D.P., Dworkin, J.P., 2012. Compound-specific carbon, nitrogen, and hydrogen isotopic ratios for amino acids in CM and CR chondrites and their use in evaluating potential formation pathways. Meteorit. Planet. Sci. 47, 1517–1536.
Elsila, J.E., Aponte, J.C., Blackmond, D.G., Burton, A.S., Dworkin, J.P., Glavin, D.P., 2016. Meteoritic amino acids: Diversity in compositions reflects parent body histories. ACS Cent. Sci. 2, 370–379.
Engel, M.H., Macko, S.A., Silfer, J.A., 1990. Carbon isotope composition of individual amino acids in the Murchison meteorite. Nature 348, 47–49.
Friedrich, J.M., McLain, H.L., Dworkin, J.P., Glavin, D.P., Towbin, W.H., Hill, M., Ebel, D.S., 2019. Effect of polychromatic X-ray microtomography imaging on the amino acid content of the Murchison CM chondrite. Meteorit. Planet. Sci. 54, 220–228.
Gilbert, A., Silvestre, V., Robins, R.J., Remaud, G.S., 2009. Accurate quantitative isotopic ^{13}C NMR spectroscopy for the determination of the intramolecular distribution of ^{13}C in glucose at natural abundance. Anal. Chem. 81, 8978–8985.
Glavin, D.P., Callahan, M.P., Dworkin, J.P., Elsila, J.E., 2010. The effects of parent body processes on amino acids in carbonaceous chondrites. Meteorit. Planet. Sci. 45, 1948–1972.
Glavin, D.P., Alexander, C.M., Aponte, J.C., Dworkin, J.P., Elsila, J.E., Yabuta, H., 2018. The origin and evolution of organic matter in carbonaceous chondrites and links to their parent bodies. Elsevier.
Glavin, D.P., Dworkin, J.P., 2009. Enrichment of the amino acid L-isovaline by aqueous alteration on CI and CM meteorite parent bodies. Proc. Natl. Acad. Sci. 106, 5487–5492.
Glavin, D.P., Elsila, J.E., McLain, H.L., Aponte, J.C., Parker, E.T., Dworkin, J.P., Hill, D. H., Connolly, H.C., Lauretta, D.S., 2020a. Extraterrestrial amino acids and L-enantiomeric excesses in the CM 2 carbonaceous chondrites Aguas Zarcas and Murchison. Meteorit. Planet. Sci. 26, 1–26.
Glavin, D.P., McLain, H.L., Dworkin, J.P., Parker, E.T., Elsila, J.E., Aponte, J.C., Simkus, D.N., Pozarycki, C.I., Graham, H.V., Nittler, L.R., Alexander, C.M.O.D., 2020b. Abundant extraterrestrial amino acids in the primitive CM carbonaceous chondrite Asuka 12236. Meteorit. Planet. Sci. 55, 1979–2006.
Hayatsu, R., Studier, M.H., Anders, E., 1971. Origin of organic matter in early solar system—IV. Amino acids: Confirmation of catalytic synthesis by mass spectrometry. Geochim. Cosmochim. Acta 35, 939–951.
Hofmann, A.E., Chimiak, L., Dallas, B., Griep-Raming, J., Juchelka, D., Makarov, A., Schwieters, J., Eiler, J.M., 2020. Using Orbitrap mass spectrometry to assess the isotopic compositions of individual compounds in mixtures. Int. J. Mass Spectrom. 457, 116410.
Huber, C., Wächtershäuser, G., 2003. Primordial reductive amination revisited. Tetrahedron Lett. 44, 1695–1697.
Jørgensen, J.K., Müller, H.S.P., Calcutt, H., Coutens, A., Drozdovskaya, M.N., Öberg, K.I., Persson, M.V., Taquet, V., van Dishoeck, E.F., Wampfler, S.F., 2018. The ALMA-PILS survey: isotopic composition of oxygen-containing complex organic molecules toward IRAS 16293–2422B. A & A 620, A170.
Koga, T., Naraoka, H., 2017. A new family of extraterrestrial amino acids in the Murchison meteorite. Sci. Rep. 7.
Kress, M.E., Tielens, A.G.G.M., 2001. The role of Fischer-Tropsch catalysis in solar nebula chemistry. Meteorit. Planet. Sci. 36, 75–91.
Lewis, C., Hilvert, D., Paneth, P., O'Leary, M.H., 1993. Carbon Kinetic Isotope Effects on the Spontaneous and Antibody-Catalyzed Decarboxylation of 5-Nitro-3-carboxybenzisoxazole. J. Am. Chem. Soc. 115, 1410–1413.
Lyons, J.R., Gharib-Nezhad, E., Ayres, T.R., 2018. A light carbon isotope composition for the Sun. Nat. Commun. 9.
Melzer, E., O'Leary, M.H., 1987. Anapleurotic CO_2 Fixation by Phosphoenolpyruvate Carboxylase in C3 Plants. Plant Physiol. 84, 58–60.
Miller, S.L., 1957. The mechanism of synthesis of amino acids by electric discharges. BBA 23, 480–489.
Monson, K.D., Hayes, J.M., 1980. Biosynthetic control of the natural abundance of carbon 13 at specific positions within fatty acids in Escherichia coli. Evidence regarding the coupling of fatty acid and phospholipid synthesis. J. Biol. Chem. 255, 11435–11441.
Muñoz Caro, G.M., Meierhenrich, U.J., Schutte, W.A., Barbier, B., Segovial, A.A., Rosenbauer, H., Thiemann, W.H.-P., Brack, A., Greenberg, J.M., 2002. Amino acids from ultraviolet irradiation of interstellar ice analogues. Nature 416, 403–406.
O'Leary, M.H., Yapp, C.J., 1978. Equilibrium Carbon Isotope Effect on a Decarboxylation Reaction. Biochem. Biophys. Res. Commun. 80, 155–160.
Öberg, K.I., 2016. Photochemistry and astrochemistry: Photochemical pathways to interstellar complex organic molecules. Chem. Rev. 116, 9631–9663.
Patel, B.H., Percivalle, C., Ritson, D.J., Duffy, C.D., Sutherland, J.D., 2015. Precursors in a Cyanosul Fi Dic Protometabolism. Nat. Chem. 7, 301–307.
Peltzer, E.T., Bada, J.L., Schlesinger, G., Miller, S.L., 1984. The chemical conditions on the parent body of the murchison meteorite: Some conclusions based on amino, hydroxy and dicarboxylic acids. Adv. Space Res. 4, 69–74.
Pietrucci, F., Aponte, J.C., Starr, R., Pérez-Villa, A., Elsila, J.E., Dworkin, J.P., Saitta, A. M., 2018. Hydrothermal decomposition of amino acids and origins of prebiotic meteoritic organic compounds. ACS Earth Space Chem. 2, 588–598.
Pizzarello, S., 2014. The nitrogen isotopic composition of meteoritic HCN. Astrophys. J. Lett. 25, 2–5.
Pizzarello, S., Krishnamurthy, R.V., Epstein, S., Cronin, J.R., 1991. Isotopic analyses of amino acids from the Murchison meteorite. Geochim. Cosmochim. Acta 55, 905–910.
Pizzarello, S., Huang, Y., Becker, L., Poreda, R.J., Nieman, R.A., Cooper, G., Williams, M., 2001. The organic content of the Tagish Lake meteorite. Science 293, 2236–2239.
Pizzarello, S., Huang, Y., Fuller, M., 2004. The carbon isotopic distribution of Murchison amino acids. Geochim. Cosmochim. Acta 68, 4963–4969.
Pizzarello, S., Cooper, G.W., Flynn, G.J., 2006. The nature and distribution of the organic material in carbonaceous chondrites and interplanetary dust particles. Meteorit. Early Sol. Syst. II 625–652.
Rasmussen, C., Hoffman, D.W., 2020. Intramolecular distribution of 13C/12C isotopes in amino acids of diverse origins. Amino Acids 52, 955–964.
Seargent, D.A., 1990. The Murchison meteorite: Circumstances of its fall. Meteoritics 25, 341–342.
Sephton, M.A., 2002. Organic compounds in carbonaceous meteorites. Nat. Prod. Rep. 19, 292–311.
Silverman, S.N., Phillips, A.A., Weiss, G.M., Wilkes, E.B., Eiler, J.M., Sessions, A.L., 2021. Practical considerations for amino acid isotope analysis. Org Geochem. 164, 104345.
Simkus, D.N., Aponte, J.C., Elsila, J.E., Parker, E.T., Glavin, D.P., Dworkin, J.P., 2019a. Methodologies for analyzing soluble organic compounds in extraterrestrial samples: Amino acids, amines, monocarboxylic acids, aldehydes, and ketones. Life 9.
Simkus, D.N., Aponte, J.C., Hilts, R.W., Elsila, J.E., Herd, C.D.K., 2019b. Compound-specific carbon isotope compositions of aldehydes and ketones in the Murchison meteorite. Meteorit. Planet. Sci. 54, 142–156.
Telus, M., Alexander, C.M.O.D., Hauri, E.H., Wang, J., 2019. Calcite and dolomite formation in the CM parent body: Insight from in situ C and O isotope analyses. Geochim. Cosmochim. Acta 260, 275–291.
Wilkes, E.B., Sessions, A.L., Zeichner, S.S., Dallas, B., Schubert, B., Jahren, A.H., Eiler, J. M., 2022. Position-specific carbon isotope analysis of serine by gas chromatography/Orbitrap mass spectrometry, and an application to plant metabolism. Rapid Commun. Mass Spectrom. 36.
Zeichner, S.S., Wilkes, E.B., Hofmann, A.E., Chimiak, L., Sessions, A.L., Makarov, A., Eiler, J.M., 2022. Methods and limitations of stable isotope measurements via direct elution of chromatographic peaks using gas chromotography-Orbitrap mass spectrometry. Int. J. Mass Spectrom. 477, 116848.

Supplemental Materials for

Position-specific carbon isotopes of Murchison amino acids elucidate extraterrestrial abiotic organic synthesis networks

S. Zeichner* et al.

*Corresponding author: S. Zeichner, szeichner@caltech.edu

This PDF file includes:

Supplemental Materials and Methods

Amino acid standards

We prepared pure amino acid standards of L+D-aspartic acid (Sigma Lots 060M0092V and MKCC0521, respectively), β-alanine (Sigma Lot BCBR6059V), and L+D α-alanine (Sigma Lots BCBF7865V, SLBN6572V, respectively). The molecular-average carbon isotopic composition of the amino acid standards were characterized by Elemental Analyzer-Isotope Ratio Mass Spectrometry (EA-IRMS) at Caltech. The mean $\delta^{13}C_{VPDB}$ values (± 1 σ_{SE}) of the aspartic acid, β-alanine, and α-alanine standards were -22.14 ± 0.07‰ (n = 3), -27.09 ± 0.40‰ (n = 3) and -19.60 ± 0.24‰ (n=3), respectively (Table S1). In addition, we prepared aspartic acid with 10% labels at each carbon site to verify which fragment ions inherit which carbon sites (gravimetrically mixed from natural abundance amino acids with >99% ^{13}C-labeled amino acids purchased from Sigma). We used a similar method to perform site assignments for β-alanine mass spectral fragments, however we were unable to acquire labeled compounds for carbon sites 2 and 3 separately, and thus had to characterize them together. (Chimiak et al., 2021) followed a similar method to characterize the fragmentation spectrum and site-assignment of α-alanine. Finally, we prepared a "meteorite standard" with 34 amino acids scaled to relative abundances of reported in (Glavin et al., 2020a) for optimizing chromatography and GC oven programs. All standards and samples were derivatized as described below.

Mass spectrometry

Overview of GC-Orbitrap mass spectrometry

Analyses were performed on a Q-Exactive Orbitrap mass spectrometer with samples introduced via a Trace 1310 gas chromatograph equipped with a TG-5SIL MS column (30 m, 0.25 mmID, 0.25 µm thickness) with a 1 m fused silica capillary pre-column (inner diameter of 220 µm/outer diameter of 363 µm, VSD tubing) (Figure 1). To perform measurements of the Winter 2022 sample, we installed two TG-5SIL MS columns connected in series with a Valco union to improve separation between our compounds of interest and near co-eluting peaks. Samples and standards were analyzed under closely matched experimental conditions.

Compounds were injected via split-splitless injector operating in splitless mode, with He as a carrier gas with a flow rate of 1.2 mL/min. The GC oven temperature program was optimized to separate the analytes of interest from the rest of the organic compounds in the extract. The mass windows for each of the mass spectral fragments measured for PSIA are presented in Figure S1. The GC has been modified through the addition of two, four-way valves and a peak-broadening reservoir, as described in Eiler et al., 2017 (Figure 1). For this study, we measured compounds in two different valve configurations: (1) "direct elution" of the GC effluent into the mass spectrometer (Zeichner et al., 2022) and (2) "peak capture" of the compound of interest within a peak-broadening reservoir (Eiler et al., 2017). Direct elution measurements were used in several ways. First, we used direct elution measurements to confirm the time of elution for each compound of interest. Direct elution measurements were also used to quantify the abundance of amino acids in both of the blanks compared to the intensity of the amino acid peaks in the sample (Table S4). Finally, direct elution measurements were critically important in detecting any potential contaminants, or near co-eluting compounds, that ionized to produce fragments within

the mass window of interest. When possible, chromatography was optimized to minimize the presence of the contaminant ions that would compete with the mass fragment we were measuring (i.e., the addition of the second column for the measurement of the Winter 2022 sample). In some cases, even with an improvement in chromatography, we could not get a clean enough mass window to perform adequate isotope ratio measurements of the fragment of interest (e.g., 198 fragment in the Winter 2022 sample). Future studies wanting to apply this technique to perform PSIA of analytes within complex sample mixtures may want to explore preparatory offline clean-up steps for their samples prior to direct elution. The potential effects of these extraneous fragment ions, and potential strategies to mitigate them are further detailed below in our discussion of "space charge effects" under *Position-specific isotope ratio analysis.*

To perform fragment isotope ratio measurements for PSIA, we used the "peak capture" method. Peak capture measurements enable the isolation of a single analyte from a complex mixture of compounds by turning valves to 'trap' the chromatographic peak of interest in a reservoir as it elutes off the GC column. Here, we used a silicon coated stainless steel reservoir (10 cc; SilcoTek, Bellefonte, PA). Following peak capture, the compound was slowly purged from the reservoir with helium over tens of minutes, permitting many different Orbitrap scans of a given sample, and thus improving the precision and accuracy of the measurement. With the peak capture method, each of our fragment ions eluted for minutes to tens of minutes, with a usable stable measurement time (i.e., the time frame where scans observed enough signal of the analyte of interest to use for isotope ratio measurement) of 3 to 10 minutes depending on the total concentration of the analyte introduced into the reservoir.

GC effluent was transferred directly into the ion source via a heated transfer line (260°C) where analytes were ionized via electron impact (EI; Thermo Scientific Extractabrite, 70eV; Fig. 1). Each compound generated a characteristic combination of fragment ions upon ionization (Figure 2), which were extracted from the source, subjected to collisional cooling during transfer through the bent flatpole, underwent mass-window selection by the Advanced Quadrupole Selector^{TM} (AQS), and were then passed through the automatic gain control (AGC) gate prior to storage in the C-trap — a potential-energy well generated by radio frequency and direct current potentials (Figure 1). Ions accumulated in the C-trap until the total charge reached a user-defined threshold (the "AGC target"), then were introduced into the Orbitrap mass analyzer as a discrete packet. Within the mass analyzer, ions orbited between a central spindle-shaped electrode and two enclosing outer bell-shaped electrodes, moving harmonically at frequencies proportional to m/z (Makarov, 2000). The raw data product of this oscillation—the "transient"—was converted via fast Fourier transform into a data product that can be processed for isotope ratio analysis (see Data processing).

We refer to each injection of a sample or standard as an "acquisition;" each acquisition is comprised of "scans," with each scan comprising ion intensities and m/z ratios averaged by the Orbitrap over a short time interval (typically 100-300 ms, where scan length is dependent on the user-defined nominal resolution setting). We refer to each set of replicate acquisitions of a fragment for both a sample and standard as an "experiment." It is critical that any application of the Orbitrap to isotope ratio analysis performs measurement under "AGC control," i.e., under conditions where the AGC target limits the number of ions admitted into the Orbitrap in each scan and is typically defined by low variation in the total ion current times the injection time (TIC*IT) over the course of a single acquisition. In our measurements, this was a constraint due to the low abundance of analyte; it was evident when the measurement when the instrument was not performing measurements under AGC control when the IT was at its maximum (3000 ms).

Position-specific isotope ratio analysis

Based on the results of labeling studies and direct elution measurements to evaluate near-coeluting peaks and the presence of contaminant ions in the system, we identified 3 target fragments for aspartic acid that independently constrain all four carbon sites (with unsubstituted masses of 113.0239 Da, 156.0272 Da, 198.0378 Da, referred to henceforth as the 113, 156 and 198 fragments) and 1 target fragment for β-alanine that constrains the amine site directly (m/z = 126.0166 Da and referred to henceforth as the 126 fragment) (Figure 2C&A). The fragment to constrain the amine site (140.0323 Da; referred to as the 140 fragment) of α-alanine was determined in a previous study (Chimiak et al., 2021) (Figure 2B).

With the Spring 2021 specimen, we measured the 113, 156 and 198 fragments of aspartic acid, and the 126 fragment of β-alanine. With the Winter 2022 specimen, we measured the 156 fragment of aspartic acid, the 126 fragment of β-alanine and the 140 fragment of α-alanine. We attempted a measurement of the 198 fragment using the Winter 2022 specimen, but noticed too much evidence of contamination from the sample matrix for the measurement to be useful. The abundance of aspartic acid in the Winter 2022 specimen was too low abundance to attain a useful measurement of the 113 fragment. Each of these fragment measurements can be translated into position-specific isotope values, as described in Section 2.5.

To measure each fragment, we first performed a direct elution measurement of a standard to confirm the timing of the compound of interest. We identified compound chromatographic peaks by when the characteristic fragment ions appeared and disappeared above baseline in the mass spectra. We chose a time window around the elution of each chromatographic peak as the part of the GC effluent to capture in the reservoir and verified this timing by "reverse peak capture" of pure amino acid standards where the effluent was routed to vent for the time frame of interest and thus verified that the compound fragment ions disappeared entirely from the mass spectrum. Generally, we turned valves to begin peak capture 15-20 seconds prior to the arrival of the peak of interest, and waited until the intensity of the peak tail returned to the baseline NL score prior to peak elution to end peak capture.

Once we verified the time window, we performed a set of peak capture measurements, alternating between measurements of sample and standard whose relative concentration were adjusted so that they had approximately the same NL score in the reservoir. Target sample sizes corresponded to ~10-50 picomoles of derivatized amino acid to achieve maximum absolute peak intensities (which are referred to within the Orbitrap software and RAW data files as "NL scores") that were >1 order of magnitude above the reservoir baseline NL score for the fragment of interest (~ $1 - 5*10^5$ for the monoisotopic peak, and $5*10^3 - 1*10^4$ for the background). Measurements of standards at different concentrations allowed us to anticipate the approximate achievable precision of a given amount of analyte, as we performed all our measurements under stable instrument conditions where achievable precision followed shot noise limits (see *Data processing*).

We selected AQS windows, resolutions, and AGC targets to achieve the maximum sensitivity for the fragment ion of interest (i.e., for the given experimental conditions, the majority of the ions being measured are the compound of interest; (Eiler et al., 2017)). However, introducing too many ions into the C-trap or the Orbitrap at once can lead to "space charge effects," a phenomenon by which ions affect the movement and trajectory of one another, disturbing them from the persistent, harmonic orbits required for Fourier-transform mass

spectrometry (Uechi and Dunbar, 1992; Gordon and Muddiman, 2001; Eiler et al., 2017; Su et al., 2017; Hoegg et al., 2018; Neubauer et al., 2018; Hofmann et al., 2020). Space charge effects can be mitigated for some cases by reducing extraneous ions in the mass window of interest so that there are fewer ions interacting with and capable of suppressing the isotope ratio of the fragments of interest (i.e., narrow the AQS window, lower the AGC target), or by reducing the length of time that the ions spend in the Orbitrap and thus the length of time they have to interact and that their harmonic orbits can inconsistently decay (i.e., lower resolution).

We performed all measurements with the narrowest AQS window that we could without introducing drops in transmission for fragments near the edge of the mass window (Eiler et al., 2017). Narrower mass windows were particularly helpful for this sample due to the complexity of the sample matrix and the large number of extraneous ions that often fell within the mass window that were not from our compound of interest. For the Spring 2021 specimen, we used AQS windows of 7 Da centered around the masses of the monoisotopic and substituted fragments of interest; for the Winter 2022 specimen we used AQS windows of 6.5 Da.

The resolution required to distinguish between the masses of closely adjacent near-isobars expected to be present in the mass spectrum can be calculated as:

$$resolution = \frac{m}{\Delta m} \ (Eqn. S1)$$

where m is the mass of an ion of interest and Δm is difference in mass necessary to separate that ion peak from an adjacent near-isobar. This required resolution is similar to the "nominal" resolution reported for the Orbitrap, which is calculated for a 200 Da fragment ion as *m/dm*, where m is mass and dm is the full peak width at half maximum intensity (FWHM). In general, sensitivity improves with lower resolution, which has also been shown to mitigate the effects of contaminants on the accuracy of isotope ratio measurements (Hofmann et al., 2020). Indeed, we did observe in preliminary experiments that with the presence of many extraneous ions within the mass window of interest, the isotope ratio of the sample relative to the standard was suppressed when we used a resolution of 120,000 instead of 60,000. All Spring 2021 sample measurements were performed with resolution of 120,000, which were measured at higher concentrations and therefore had fewer issues with contaminant ions of a similar concentration to the fragment ions of interest. All of the results we report from Winter 2022 analyses were performed using a resolution of 60,000.

The choice of AGC target was directly related to the relative abundance of the fragment of interest. Measurements of larger fragments with cleaner mass windows were performed with AGC targets of $2*10^5$; smaller fragments (i.e., 113 fragment of aspartic acid) that may be more susceptible to space charge effects were measured using an AGC target of $5*10^4$. All acquisitions for a single experiment were performed using the same parameters. A full set of experimental conditions used for each experiment is included in Table S3.

Data analysis

Data processing

Data files from each acquisition are converted to selected-mass chromatograms (intensity versus time for a selected m/z) which can then be integrated to yield isotope ratios. We used *FT Statistic,* a computer program written by ThermoFisher™, to extract data from RAW files created by the proprietary Orbitrap control software. From the *FT Statistic*-processed files, we extracted ion intensities (NL scores), peak noise, total ion current (TIC), injection time (IT), and other acquisition statistics, which we analyzed via in-house code written in Python (version 3.7.6). Definitions of each of these parameters can be found in prior Orbitrap studies (e.g., (Eiler et al., 2017)). The data analysis process is described in the subsequent paragraphs, and the processing code can be found on the Caltech data repository (Zeichner, 2021). Raw data for samples and standards were processed identically to enable comparisons between measurements, and is available in an online repository: https://doi.org/10.5281/zenodo.7549008.

We went through the raw files for each acquisition of an experiment to identify a consistent time frame of integration where the Orbitrap mass analyzer was operating under AGC control. We identified this time frame based on when the IT time was < 3000 ms, or the maximum IT time. As a secondary check on AGC control, we confirmed that the TIC*IT variation was < 20% for all the scans used in our isotope ratio analysis. In many cases, different acquisitions of a given experiment stayed under AGC control for different lengths of time, likely due to minor inconsistencies in the overall abundance in analyte concentration from acquisition to acquisition. We used the most conservative (i.e., shortest) time frame for all acquisitions within an experiment. Prior studies that have used the Orbitrap to perform isotope ratio measurements have used a NL score-based culling threshold of 10% to decide which scans to use in isotope ratio measurements (Zeichner et al., 2022; Wilkes et al., 2022). However, we noticed that this threshold was not as applicable to the study of such small sample sizes; the time frame where our measurement of fragment ions by reservoir elution left AGC control ranged in what the intensity of the unsubstituted fragment was relative to the total ion current (NL score/TIC; e.g., 3-40%). For cases where the NL score / TIC < 5% when the measurement was no longer under AGC control, we used a 5% baseline as a cutoff.

We explored the use of baseline corrections for our measurements. In all cases, the baseline for the Murchison sample was higher than the standard, and so we expect that baseline subtraction would increase the isotope ratio of our samples relative to our standards. However, to perform adequate baseline corrections, it is critical to measure the background under AGC control. The background was only observed under AGC control for one experiment—the measurement of the 126 fragment—and otherwise the background prior to the elution of the analyte peak out of the reservoir was observed under conditions of maximum IT. We perform a background correction for the 126 fragment, where we subtract an average of the NL score for unsubstituted and the substituted fragment ion masses during the background scans from each of the scans selected within our chosen time frame for data analysis, prior to conversion to ion counts, described below. Note that the incorporation of this background correction for the 126 fragment measurement did increase the σ_{SE} due to having fewer counts to quantify and use in the computation of the isotope ratio of the fragment. For all other fragments, we report the relative height of the NL score of the background to that of the eluting peak (Table S3), but do not perform any quantitative baseline correction.

Raw data files report signal intensities, which must be converted into the number of ions ('ion counts') to compute isotope ratios. To calculate isotope ratios for each chromatographic peak, we next converted NL scores for each remaining scan into ion counts (Eiler et al., 2017):

$$N_{io} = \frac{S}{N} * \frac{C_N}{z} * \sqrt{\frac{R_N}{R}} * \sqrt{\mu}\ (Eqn.S2),$$

where N_{io} is the number of observed ions, S is the reported signal intensity (NL score) for the molecular or fragment ion in question, N is the noise associated with that signal, R is the formal resolution setting (defined for m/z 200) used, R_N is a reference formal mass resolution at which eqn.2 was established, C_N is the number of charges corresponding to the noise at reference resolution R_N (4.4; a constant established by prior experiments; see Eiler et al., 2017), z is the charge per ion for the fragment of interest, and μ is the number of microscans (i.e., sequential Orbitrap ion packet injections that were averaged, analyzed by fast-Fourier transform, and reported as a single scan).

To compute isotope ratios, we take scans where the monoisotopic peak intensity (NL score) is under AGC control, as described above. The unsubstituted and monoisotopic ions in the remaining scans were respectively summed, and then divided to calculate the isotope ratio of interest. We report both fragment and position-specific isotope ratios in the common "delta" (δ) notation (Equation 1). We explicitly state the reference frame for each reported value and use subscripts on delta values to denote the compound or carbon position for which the isotope value is being reported. With our delta values, we report the standard error for isotope ratio measurements across replicate acquisitions ($\sigma_{SE;}$ Equation 7). Both σ and σ_{SE} are reported in per-mille (‰).To refer to σ_{SE} of specific fragments, "f", we refer to them as σ_{SE-f}.

We compare our achieved σ_{SE} with the theoretical "shot noise limit" of each acquisition based on the number of observed counts:

$$\frac{\sigma_{SNL}}{R} = \sqrt{\frac{1}{\sum C_{io}} + \frac{1}{\sum c_{io}}}\ (Eqn.S3),$$

where $\frac{\sigma_{SNL}}{R}$ is the shot noise limit on a single acquisition, which is calculated based on $\sum C_{io}$ and $\sum c_{io}$ — the sums of all the counts for the substituted and unsubstituted molecular or fragment ions of interest, respectively. The shot noise limits represent the best-case uncertainty on a measurement of the *N/n* ratio and serves as a useful point of comparison with acquisition errors and experimental reproducibility, σ and σ_{RSE}, as defined above.

Fragments constraining other molecular positions

We attempted to measure two additional fragments: a 138.01607 Da fragment of aspartic acid that would allow us independently constrain the isotope values of the methylene and second carboxyl sites, and a 70.082874 and 139.0238 Da fragment of β-alanine that would allow us to constrain the isotope value of the methylene and carboxyl (C1+C2) carbon sites together. However, these masses fell within mass windows that often had fragments from other co-eluting and near-co-eluting compounds. It was impossible to get an adequately clean mass window for suitable isotope ratio measurements of these fragments (i.e., mass windows where there were not prominent (>20% of the NL score of the base peak) contaminant fragment ions), but future studies may be able to achieve this measurement with improved chromatography or offline preparatory separation steps.

The matrices used and equations used for these position-specific computations for all three compounds are depicted in Figure S2. Figure S2 also includes additional equations that could be

used to constrain all of the carbon sites in each molecule, given additional measurements of 138 Da fragment of aspartic acid, 70 and 139 Da fragments of β-alanine and the 184 fragment of α-alanine.

Error propagation

Because each position-specific isotope value is measured indirectly, we must propagate the errors from fragment isotope ratio measurements, which we did for each fragment of aspartic acid as follows:

$$\sigma_{SE-C1}=\sqrt{(5*\sigma_{SE-113})^2+(6*\sigma_{SE-198})^2}\ (Eqn.S4)$$

$$\sigma_{SE-C2}=4*\sigma_{SE-113}\ (Eqn.S5)$$

$$\sigma_{SE-C3+C4}=\sqrt{(6*\sigma_{SE-198})^2+(4*\sigma_{SE-156})^2}\ (Eqn.S6)$$

We note that errors on our position-specific isotope ratios are correlated due to the use of each fragment measurement in multiple calculation. Errors on the position-specific carbon isotope value of the amine (C3) carbon of β-alanine was calculated as follows:

$$\sigma_{SE-C3}=3*\sigma_{SE-126}\ (Eqn.S7)$$

To compute the error on the position-specific carbon isotope value of the amine carbon (C2) of α-alanine, we added errors reported by (Chimiak et al., 2021)with propagated errors from our 140 fragment measurements of the sample and standards added in quadrature as follows:

$$\sigma_{SE-C2}=\sigma_{SE-C3,Chimiak}+4*\sqrt{(\sigma_{SE-140-standard})^2+(\sigma_{SE-140-sample})^2}\ (Eqn.S8)$$

Supplemental References

Gordon E. F. and Muddiman D. C., 2001. Impact of ion cloud densities on the measurement of relative ion abundances in fourier transform ion cyclotron resonance mass spectrometry: Experimental observations of coulombically induced cyclotron radius perturbations and ion cloud dephasing rates. J. Mass Spectrom. 36, 195–203.

Hoegg E. D., Marcus R. K., Hager G. J., Hart G. L. and Koppenaal D. W., 2018. Concomitant ion effects on isotope ratio measurements with liquid sampling-atmospheric pressure glow discharge ion source Orbitrap mass spectrometry. J Anal At Spectrom 33, 251–259.

Makarov A., 2000. Electrostatic Axially Harmonic Orbital Trapping: A High-Performance Technique of Mass Analysis. Anal Chem 7, 1156-1162.

Neubauer C., Sweredoski M. J., Moradian A., Newman D. K., Robins R. J., Eiler J. M. and A, 2018. Scanning the isotopic structure of molecules by tandem mass spectrometry. Int J Mass Spectrom 434, 276-286.

Su X., Lu W. and Rabinowitz J. D., 2017. Metabolite spectral accuracy on Orbitraps. Anal Chem 89, 5940–5948.

Uechi G. T. and Dunbar R. C., 1992. Space charge effects on relative peak heights in Fourier transform-ion cyclotron resonance spectra. J. Am. Soc. Mass. Spectrom. 3, 734–741.

Zeichner S., 2021. caltechorbi/OrbitrapDataProcessing: orbicodeV1.0.3. https://doi.org/10.22002/D1.2170

Figure S1. Mass windows of measured mass spectral fragments. Peak capture experiments measured narrowed mass windows centered around the unsubstituted mass fragment of interest.

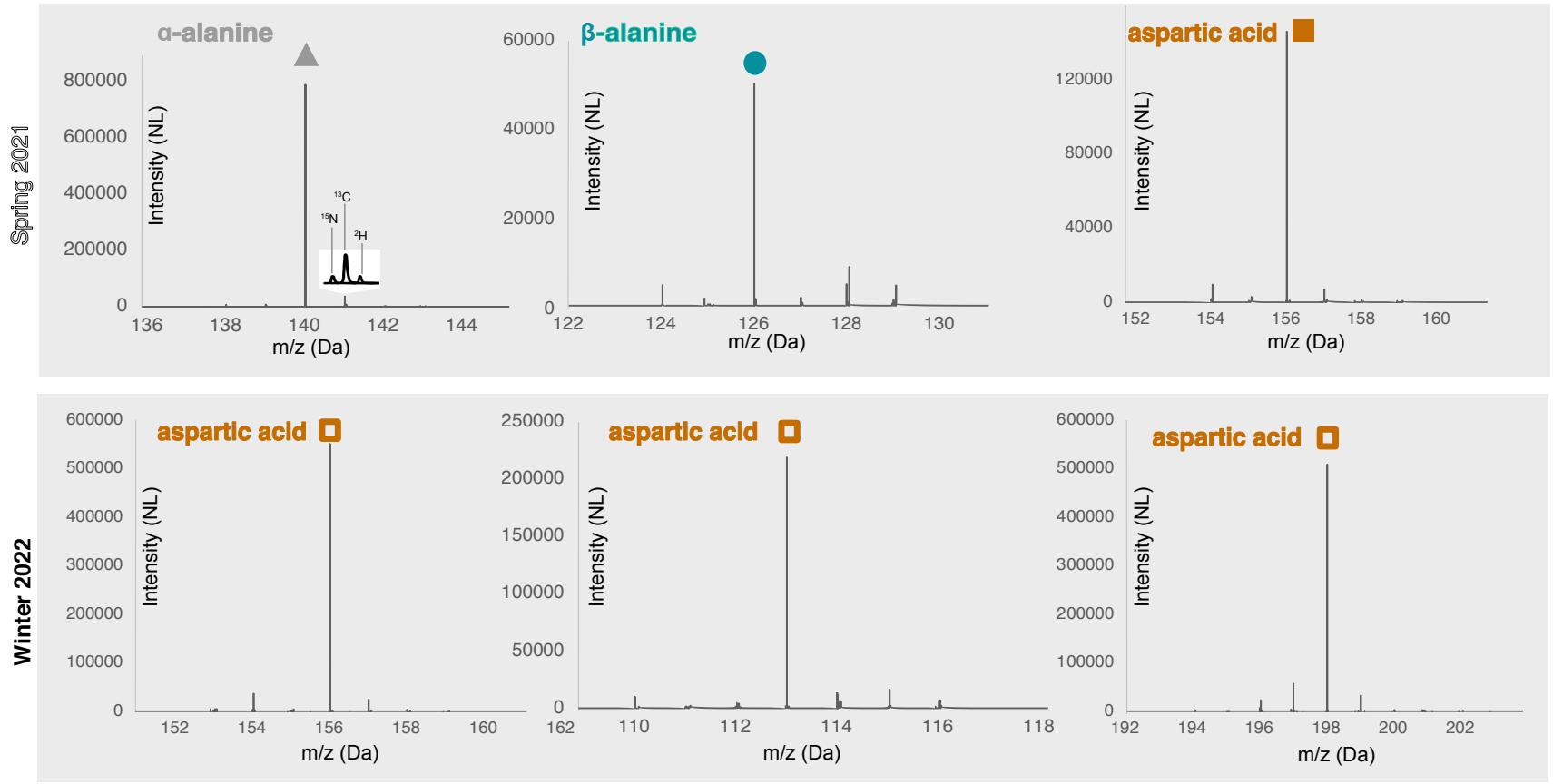

Figure S2. Matrix math and equations to compute position-specific $\delta^{13}C_{PDB}$ values. (A) Aspartic acid matrix math and equations. (B) β-alanine matrix math and equations. (C) α-alanine matrix math and equations. All equations are written to compute full conversion of position-specific isotope values within mPDB* space (computed by adding the $\delta^{13}C_{PDB}$ value of the house standard, included in the upper right corner of each panel in blue). Properties and equations used in this study are bolded and in black; other equations that could be used to fully constrain all sites of each molecule are included for completeness but in grey.

A Aspartic acid — $\delta^{13}C_{std, PDB}$ = -22

C1	C2	C3	C4	A	B	C
0	¼	0	0	¼	¼	¼
1/5	1/5	1/5	1/5	1/5	0	0
0	¼	¼	0	0	¼	¼
0	1/6	1/6	1/6	1/6	1/6	1/6
0	0	0	0	1	0	0
0	0	0	0	0	½	½
0	0	0	0	0	1	-1

X

C1	156
C2	113
C3	138
C4	198
A	MeOH
B	TFA
B	TFA

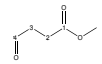
113

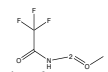
156

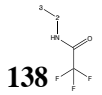
138

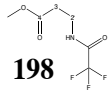
198

C1 = $5F_{113} - 6F_{198} + \delta^{13}C_{std, PDB}$
C2 = $4F_{156} + \delta^{13}C_{std, PDB}$
C3 = $4F_{138} - 4F_{156} + \delta^{13}C_{std, PDB}$
C4 = $6F_{198} - 4F_{138} + \delta^{13}C_{std, PDB}$
Avg(C3+C4) = $\left(\frac{6*\delta^{13}C_{198} - 4*\delta^{13}C_{156}}{2}\right) + \delta^{13}C_{std, PDB}$

B β-alanine — $\delta^{13}C_{std, PDB}$ = -27

C1	C2	C3	A	B	C
1/3	1/3	1/3	0	0	0
0	0	1/3	0	1/3	1/3
0	¼	¼	0	¼	¼
0	0	0	1	0	0
0	0	0	0	½	½
0	0	0	0	1	-1

X

C1	70
C2	126
C3	139
A	MeOH
B	TFA
C	TFA

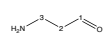
70

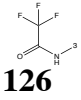
126

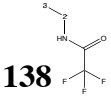
138

C1 = $3C_{70} - 4F_{139} + 3F_{126} + \delta^{13}C_{std, PDB}$
C2 = $4F_{139} - 3F_{126} + \delta^{13}C_{std, PDB}$
C3 = $3F_{126} + \delta^{13}C_{std, PDB}$

C α-alanine — $\delta^{13}C_{std, PDB}$ = -19

C1	C2	C3	A	B	C
0	¼	¼	¼	¼	0
1/5	1/5	0	1/5	1/5	1/5
1/3	1/3	1/3	0	0	0
0	0	0	1	0	0
0	0	0	0	½	½
0	0	0	0	1	-1

X

C1	140
C2	184
C3	Molecular average (MA)
A	MeOH
B	TFA
C	TFA

C1+ C2 +C3 = MA
C2 +C3 = $4F_{140}$
C1 +C2 = $5F_{184}$
C2 = ($4F_{140}$ $- (\delta^{13}C_{C3,PDB*} - \delta^{13}C_{std,PDB})$) $+ \delta^{13}C_{std, PDB}$

**From Chimiak et al., 2021,* $\delta^{13}C_{C3, PDB}$ = -36

Table S1. Mass spectral fragment isotope ratios and delta values. Mass spectral fragment isotope ratios for aspartic acid, β-alanine and α-alanine from Murchison, reported as both $R_{sample}/R_{standard}$ and $\delta^{13}C_{house\ standard}$. Values are reported along with molecular average $\delta^{13}C_{VPDB}$ of amino acid standards, measured by EA. Reported errors are $1\sigma_{SE}$.

	standard $\delta^{13}C \pm \sigma_{SE}$ (‰, VPDB)	**Fragment**	**Specimen**	**Carbon sites**	**R_{sample}/R_{std} (σ_{SE})**	**Murchison $\delta^{13}C \pm \sigma_{SE}$ (‰, house standard)**
Aspartic acid	-22.14±0.07	113	Spring 21	A,B,C,D	1.0055 (0.004)	5.5±4.1
		156	Spring 21	B	1.0033 (0.002)	3.3±2.4
		156	Winter 22	B	1.0020 (0.001)	2.0±1.4
		198	Spring 21	C,D	0.9987 (0.002)	-1.3±2.3
β-Alanine	-27.09±0.04	126	Winter 22	B	1.020 (0.008)	20.1±7.9
α-Alanine	-19.60±0.24	140	Winter 22	A,B	1.028 (0.0003)	27.7±1.2

Table S2. Position-specific carbon isotope ratios. Delta values are reported both relative to our house amino acid standards as well as converted to our mPDB* reference frame. Reported errors are propagated σ_{SE}.

Carbon letter	**Specimen**	**Carboxyl 1**			**Amine**			**Average of Methylene + carboxyl 2**		
		$\delta^{13}C$ (‰, vs std)	**$\delta^{13}C$ (‰, mPDB*)**	**σ_{SE}**	**$\delta^{13}C$ (‰, vs std)**	**$\delta^{13}C$ (‰, mPDB*)**	**σ_{SE}**	**$\delta^{13}C$ (‰, vs std)**	**$\delta^{13}C$ (‰, mPDB*)**	**σ_{SE}**
Aspartic acid	Winter 22	-		-	7	-14	5	-		-
	Spring 21	35	13	25	13	-9	10	-10	-32	17
β-alanine	Winter 22	-		-	60	33	24	-		-
α-alanine	Winter 22				128	109	20			

Table S3. Experimental conditions for Spring 2021 and Winter 2022 specimens.

Specimen, Date of measurement	Compound	Fragment	Orbitrap parameters (AGC target, resolution, AQS window)	Valve turn timing	Peak integration timing	Background timing (if applicable)	Maximum NL score (NL score of background)
Spring 2021, 4/29/2021	Aspartic acid	156	$2*10^5$, 120,000, 153 to 160	18.05 to 19.6	18.7 to 24.5	n/a	$5*10^5$ ($5*10^3$)
Spring 2021, 4/30/2021	Aspartic acid	113	$5*10^4$, 120,000, 153 to 160	18.05 to 19.6	18.7 to 26.7	n/a	$2*10^5$ ($8*10^3$)
Spring 2021, 5/3/2021	Aspartic acid	198	$2*10^5$, 120,000, 153 to 160	18.05 to 19.6	18.7 to 25	n/a	$5*10^5$ ($5*10^3$)
Winter 2022, 1/31/2022	Aspartic acid	156	$2*10^5$, 60,000, 153.5 to 159.5	36.4 to 36.75	36.7 to 41.3	n/a	$1.5*10^5$ ($3.93*10^3$)
Winter 2022, 2/3/2022	β-Alanine	126	$2*10^5$, 60,000, 123.5 to 129.5	19.3 to 20.2	19.7 to 39	19.4 to 19.55	$3.12*10^5$ ($1.14*10^4$)
Winter 2022, 2/3/2022	α-Alanine	140	$2*10^5$, 60,000, 137.5 to 144.5	13.6 to 14.3	13.99 to 26.3	n/a	$5*10^5$ ($8*10^3$)

Table S4. Blanks.

	Retention time	Murchison, NL score	GSFC Blank, NL score	Caltech Blank, NL score
α-Alanine	13.74	$2.21*10^8$	$3.45*10^5$	$<1*10^4$
β-Alanine	19.61	$2*10^7$	$<1*10^4$	$<1*10^4$
Aspartic acid	36.9	$1.1*10^6$	$3*10^4$	$<1*10^4$

Table S5. Prior compound specific carbon isotope values of Murchison amino acids. Note that the reported range of values for each compound may reflect heterogeneities or some terrestrial contamination.

Amino acid	$\delta^{13}C$ (‰, VPBD)	Reference
α-Alanine	+51.7±1.9 (D), +38.5±(2.2)	(Pizzarello et al., 2004)
	38±10 (D), 40±19 (L)	(Elsila et al., 2012)
	+49±5 (D), +38±5 (L)	(Glavin et al., 2020a)
	+25.5±3	(Chimiak et al., 2021)
	+30 (D), +27 (L)	(Engel et al., 1990)
	+52 (D), +38 (L)	(Engel et al., 1990)
Aspartic acid	+25.2 (D), -6.2 (L)	(Pizzarello et al., 2004)
	+4	(Pizzarello et al., 1991)
β-Alanine	+4.9±0.5	(Pizzarello et al., 2004)
	+10±6	(Elsila et al., 2012)
	+10±1	(Glavin et al., 2020a)
	+5	(Pizzarello et al., 2006)

Table S6. Prior compound specific carbon isotope values of putative organic precursor and intermediate compounds.

	Compound	$\delta^{13}C$ (‰, VPBD)	Reference
Murchison and Murchison parent body	Butyric acid	+11	(Pizzarello et al., 2006)
	Carbon monoxide	-32	(Pizzarello et al., 2006)
	Carbon dioxide	+29.1	(Pizzarello et al., 2006)
	KCN	+5±3	(Pizzarello, 2014)
	Dicarboxylic and hydroxy dicarboxylic acid, Murchison	-6	(Cronin et al., 1993)
Cometary	HCN	+16 (+262, -172‰)	(Cordiner et al., 2019)
Interstellar	CO	+110 to +160‰	(Lyons et al., 2018; Chimiak et al., 2021)